PREVENTION OF MYOCARDIAL INFARCTIONS, USING NON INVASIVE BIOPHOTONICS MEASUREMENT OF BIOMARKER CARDIAC TROPONIN I

by

Sara Moghaddamjoo
Honours BASc, Simon Fraser University, 2009

THESIS SUBMITTED IN PARTIAL FULFILLMENT OF
THE REQUIREMENTS FOR THE DEGREE OF

MASTER OF APPLIED SCIENCES

In the
School of Engineering Science

SIMON FRASER UNIVERSITY

Fall 2010

APPROVAL

Name:	**Sara Moghaddamjoo**
Degree:	**Master of Applied Sciences**
Title of Thesis:	**Prevention of Myocardial Infarctions, Using Non-Invasive Biophotonics Measurement of Biomarker Cardiac Troponin I.**

Examining Committee:

Chair: _____

Dr. Ash Parameswaran, P. Eng.
Professor, School of Engineering Science

_____

Dr. Andrew Rawicz, P. Eng.
Senior Supervisor
Professor, School of Engineering Science

_____

Dr. Glenn Chapman, P. Eng.
Supervisor
Professor, School of Engineering Science

_____

Dr. Glen Tibbits,
Internal Examiner
Professor, Department of Biomedical Physiology and Kinesiology

Date Defended/Approved: _____

ABSTRACT

Coronary Heart Disease is the leading cause of death worldwide. Myocardial Infarctions are one of the most frequent cardiovascular diseases. The aim of this research is to design a non-invasive heart attack detection system based on biphotonic measurements. Several methods such as ECG monitoring, Florescence and Raman Spectroscopy are evaluated and Raman Spectroscopy is chosen due to advantages in sensitivity and efficiency. Since cTnI test is the current gold standard in diagnosing MI, the initial part of this research is based on a comprehensive study of this protein. In this research Raman spectra of cTnI is measured and after assessment of possible adjustments to noise level, SERS method is used to obtain the enhanced spectra and consequently a unique cTnI Raman signature. Due to low biological concentrations and low SNR, the spectra are measured in higher concentrations. Finally, a conceptual Raman design is proposed as a part of the instrumentation study of the system.

Keywords: Biophotonics, Spectroscopy, Raman Spectroscopy, Cardiac Biomarkers, Cardiac Troponin I, Myocardial Infarction.

EXECUTIVE SUMMARY

Despite the presence of numerous preventive public-health measures directed at decreasing incidences of cardiovascular morbidity and mortality, Coronary Heart Disease (CHD) remains the leading cause of death worldwide. Myocardial Infarctions, or heart attacks, are one of the most frequent cardiovascular diseases as epidemiologic reports suggest that on average one out of six patients with a heart attack die within 30 days of the event; such mortality rates are exceedingly higher if the patient has had a history of other co-morbidities which are often the case. Such high mortality rates are often associated with late diagnosis, therapeutic intervention, meaning significant physiologic stress has been imposed on the patient's cardiovascular system by the time they reach the hospital, and the repercussions are simply irreversible, leading to death or permanent debilitations. Even though heart attacks naturally occur suddenly, minor physiological changes gradually take place a few hours prior to the "attack". Such physiological changes involve the release of very low concentrations of well described biomarkers. These extensively studied and specific biomarkers are released into the circulatory system due to myocardial tissue death and this process is initiated well before the onset of the attack. Cardiac Troponin I (cTnI) is considered one of the most specific and widely used cardiac biomarkers. While cTnI concentrations are routinely clinically used to confirm the diagnosis of a heart attack once the patient arrives at the E.R, current technology limits medical detection of only "post-attack" biomarker concentrations in the circulation. Unfortunately, at this point, the physiological damages are often irreversible.

The purpose of this research is to design a real-time intelligent system, using a miniaturized Raman spectroscope, for detection of early heart attack using non-invasive biophotonic measurements. This technology is aimed at detecting very low concentrations of cardiac biomarkers so that the patient becomes aware of real time damage to the myocardial tissue and hence can seek medical attention well before significant and irreversible damage is imposed on the heart. Our proposed measurement site is the circulatory system posterior to the retina and the small detection device will be implanted on spectacle frames to make continuous real time measurement through the patient's eye. Therefore, high-risk individuals can simply wear their "glasses" and rest assured that they are constantly being screened for elevated circulating biomarker concentrations that imply ongoing myocardial damage.

Prior to using Raman Spectroscopy, we have used Florescence Spectroscopy to obtain preliminary information on cTnI in order to further characterize this protein. So far, we have been collaborating with Grant Group Laboratory at the department of chemistry at University of British Columbia, and Cardiac Physiology Group Laboratory at Simon Fraser University. Through such collaborations, we were able to characterize the unique Raman signature of cTnI for the very first time based on existing literature. The major challenge of this research is of course the very low concentrations of this biomarker in the blood prior to irreversible damage. Currently, this limitation does not allow for measurement of cTnI protein at biological concentration levels using our available detectors. This constraint can be resolved by using EMCCD detector in the future. Moreover, in parallel with the analytical portion of the research, we worked on

the instrumentation with the purpose of designing a small Raman spectrometer, which can be attached to spectacle frames.

In conclusion, our preliminary results strongly suggest that continuation of this research by increasing the sensitivity of cTnI Raman signal acquisition and designing the medical device instrumentation is worthwhile and valuable in the field of non-invasive diagnosis and has the potential to substantially decrease the number of cardiovascular morbidity and mortalities.

ACKNOWLEDGEMENTS

I would like to thank Dr Andrew Rawicz for his continuous supervision and mentorship from the beginning of my studies at SFU. Without his help and motivation, none of my achievements were possible. This study was prepared in collaboration with Grant Group at the University of British Columbia and Molecular Cardiac Physiology Group at Simon Fraser University. I would like to thank Professor Glen Tibbits, Professor Glenn Chapman, Professor Edward Grant, Dr Marinko Sarunic, Dr Michael Chen and their students and researchers for valuable contribution to this research. Moreover, this research could not be possible without the help of my friend and fellow graduate researchers in this project, Mr Pasha Tashakor. I would also like to thank my family and friends for their support and encouragement.

TABLE OF CONTENTS

LIST OF FIGURES

LIST OF TABLES

GLOSSARY

APD	**Avalanche photo diode**
AMI	Acute Myocardial Infarction
Asp	Aspartic acid
BP	Bandpass Filter
BSA	Bovine Serum Albumin
BS	Beam Splitter
CCD	Charged Coupled Device
CW	Continuous Wavelength
cSLO	Confocal Scanning Laser Ophthalmoscopy
cTnC	Cardiac Troponin C
cTnI	Cardiac Troponin I
cTnT	Cardiac Troponin T
DG	Diffraction Grating
DM	Dichroic Mirror
ECG	Electrocardiogram
ELISA	Enzyme-Linked Immunosorbent Assay
F	Phenylalanine
Glu	Glutamine
HCl	Hydrochloric Acid
LPDF	Long Pass Dichroic Filter
PCB	Printed Circuit Board
PLS	partial least-squares
PMT	Photo Multiplier Tube
SG	Savitzky–Golay (SG)
SLO	Scanning Laser Ophthalmoscopy
SNR	signal-to-noise Ratio
TMB	Tetramethyl benzidine
ULRR	Upper Limit of Reference Range
W	Tryptophan
Y	Tyrosine

1: INTRODUCTION AND BACKGROUND INFORMATION

1.1 Introduction

The 2002 World Health Organization report revealed that 59% of all deaths in that year were due to non-communal diseases. Furthermore 29% of all deaths were related to cardiovascular complications. This corresponds to approximately 10 million deaths per year resulting from cardiovascular complications [1]. Even though it is generally perceived that the elderly are more prone to heart attacks, many cardiovascular diseases are hereditary. Therefore, young adults as well as the elderly might be at risk and must take necessary precautions to prevent or reduce such incidents. Despite the development of many methods to reduce the severity or frequency of heart attacks, it is still the leading cause of death. Most heart attacks could be somewhat maintained if the patient is to receive the needed medical attention in time.

In the USA, missed myocardial infarction (MI) is the leading subject of medical malpractice claims against hospital emergency rooms and primary care physicians [2]. On the other hand, admission of patients with a low probability of acute coronary artery disease often leads to excessive and unnecessary hospital costs [2]. thank

The presented study investigates the feasibility and possibility of a non-invasive heart attack prevention system. The long-term purpose of this project is to design a real-time system for detection of heart attack using non-invasive biophotonic measurements. Figure 1 presents admission charts of patients with suspected cardiac damage at the hospital. It can be noted from the figure that Troponin tests play an important role in determining the level of MI risk. Cardiac Troponin I (cTnI) is a cardiac specific protein, which is released into blood stream soon after onset of cardiac damage.

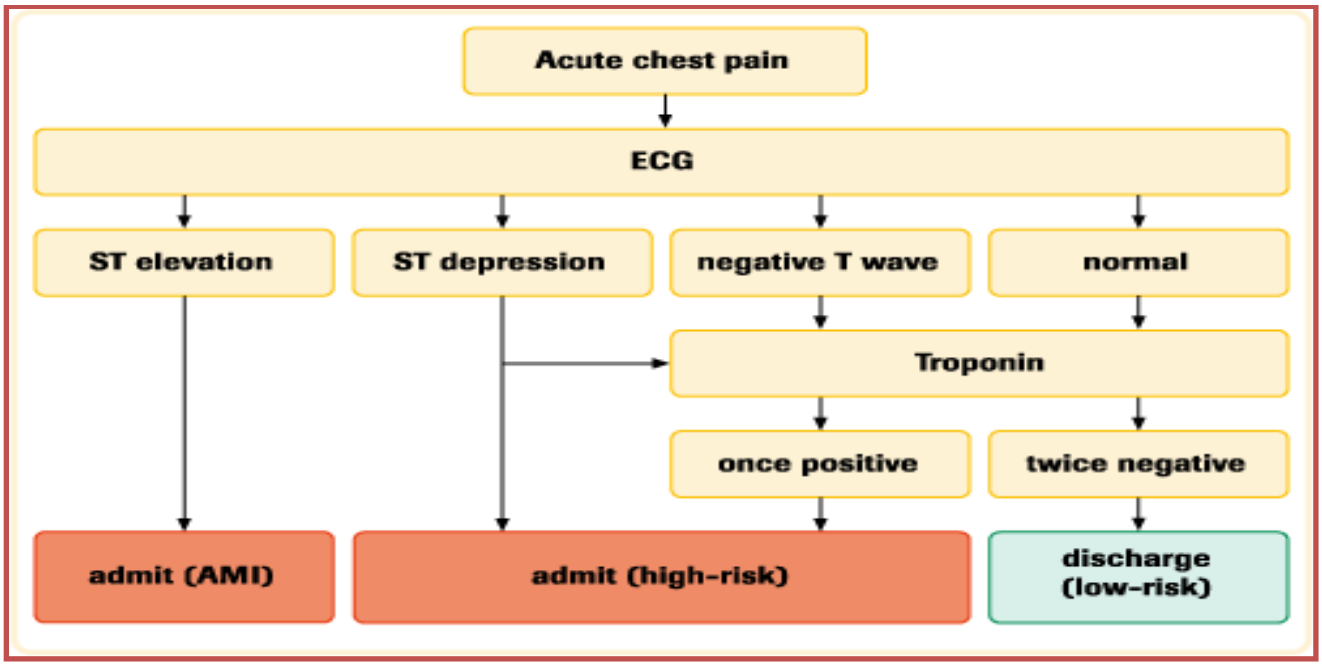

Figure 1: Admission Charts of Patients with Suspected Cardiac Damage (Modified from [2]).

The initial study to investigate the possibility of heart attack detection was conducted based on monitoring Electrocardiogram (ECG) signals. The following section describes this system.

1.2 Wireless ECG Monitor

Telemedicine is a new advancement in the delivery of clinical care through information technology and communication devices. This technology could be used immensely for disease detection and therapeutic purposes. It has been proven that early detection of a disease at its preliminary stages could profoundly reduce the risks and complications that may arise with time.

Electrocardiogram (ECG) measures the electrical activity of heart beats that generate a wave or impulse through the heart muscles. This electrical impulse would constrict the cardiac muscles which in turn cause blood to be pumped out of the heart and into the arteries. By knowing the length of time required for an electrical wave to travel through the heart, ECG

allows physicians to determine whether the electrical activity is normal, too fast/slow or irregular, for patience with cardiac issues.

An ECG can also give information about the size and health-state of the heart based on the amount of electrical activity that passes through the heart muscle. Based on these types of information, an ECG analysis can detect a heart attack.

1.2.1 System Overview

The aim of this section of the project was to enhance the ECG technology to allow early detection of heart attack as soon as soon as it is experienced by the patient. By taking advantage of one of the communication technologies that is available today, namely, Bluetooth, the aim was to design and implement a device that can be easily worn as an accessory to monitor the heart beat. The data is monitored in this system in real time and as soon as an abnormality in heart beat is detected, the data is transmitted to the patient's cell phone via a Bluetooth connection. Subsequently an emergency alarm is transmitted to another server, for example the emergency phone line, alerting professional health-care personnel. Figure 2 shows the overview of the latter system.

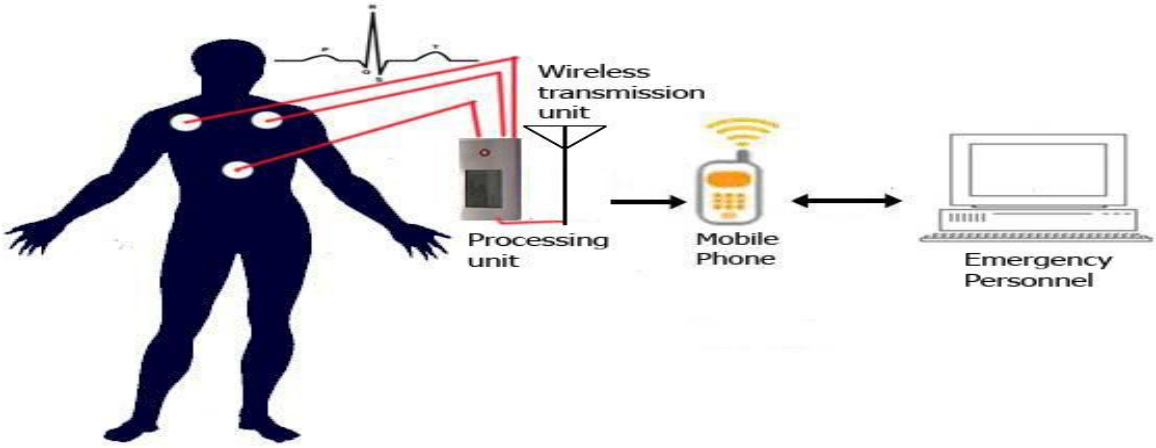

Figure 2: Wireless ECG Monitor System Overview

The heart signal was captured via ECG sensors using a biological signal acquisition circuitry; noise reduction was applied, followed by signal amplification. The amplified signal was digitized and processed via a microprocessor. In the next step, signal conditioning was applied to detect any abnormality of the heart signal. If an abnormality was detected, a signal was transmitted to a mobile phone via Bluetooth technology. The mobile phone in turn would alert appropriate agencies. Figure 3 demonstrates a block diagram of the System.

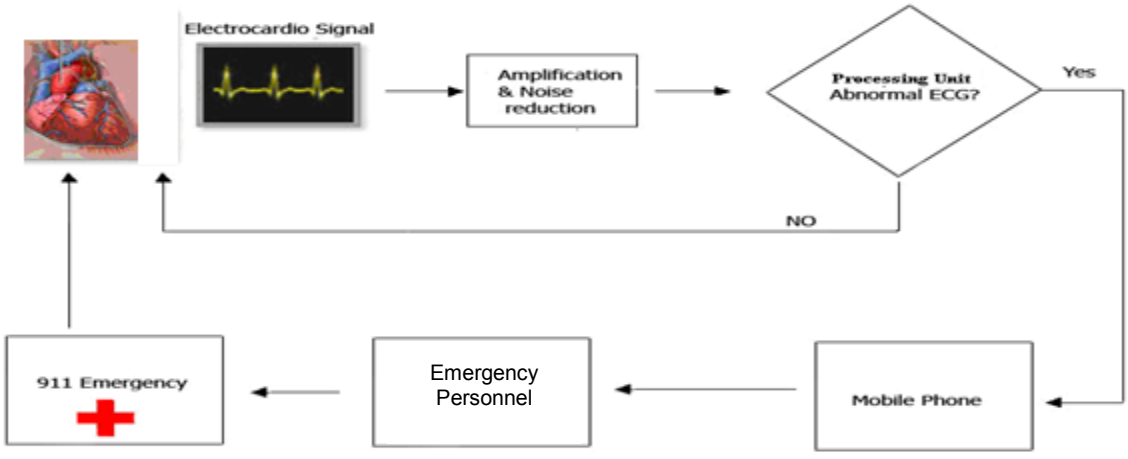

Figure 3: Wireless ECG Monitor System Block Diagram

1.2.2 Prototype Design

As described in the system overview, the system is composed of various parts. The overall system component of the ECG monitor system is presented in Figure 4.

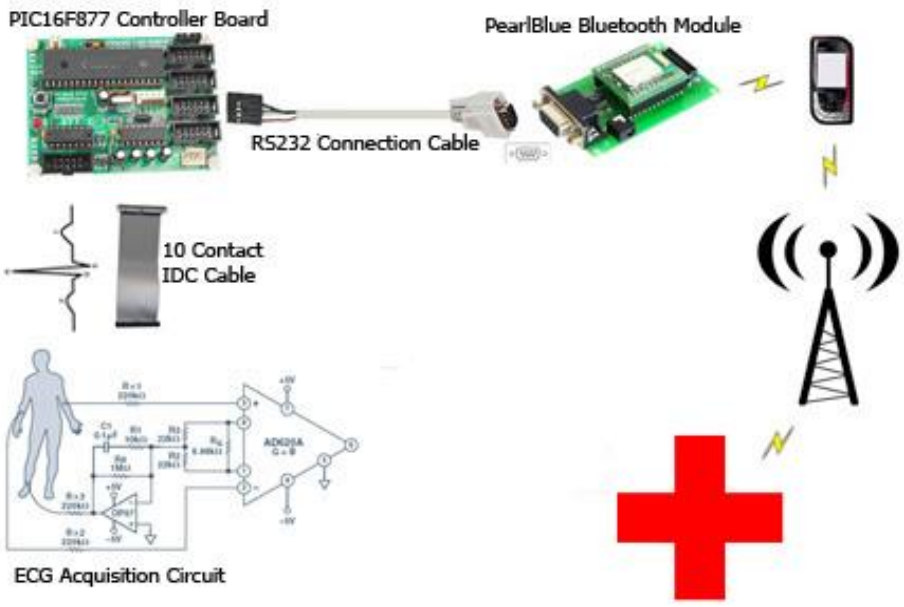

Figure 4: Wireless ECG Monitor System Components (Modified from [3])

Figure 5 illustrates the circuit design of ECG signal acquisition circuit and Figure 6 presents the PCB design of the signal acquisition circuit.

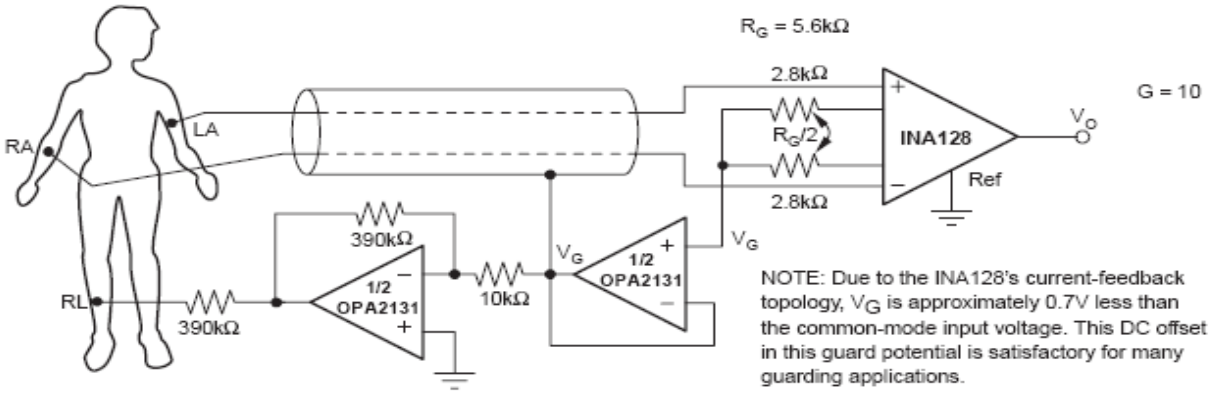

Figure 5: Wireless ECG Monitor Data Acquisition circuit using INA128 (Modified from [3])

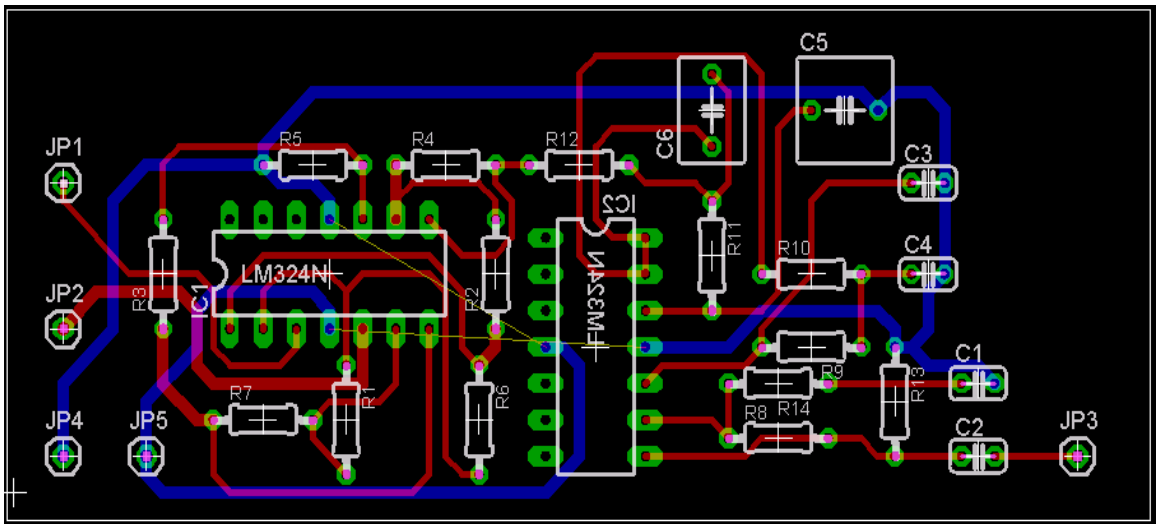

Figure 6: PCB Design of the Overall Signal Acquisition Circuit

The system was designed to detect a heart abnormality condition called ST elevation from the ECG signal. Normal and abnormal ECG test signals were generated with LabView™ software. A screen capture of these signals is shown in Figure 7. Figure 8 represents a preliminary sketch of the front view of the device.

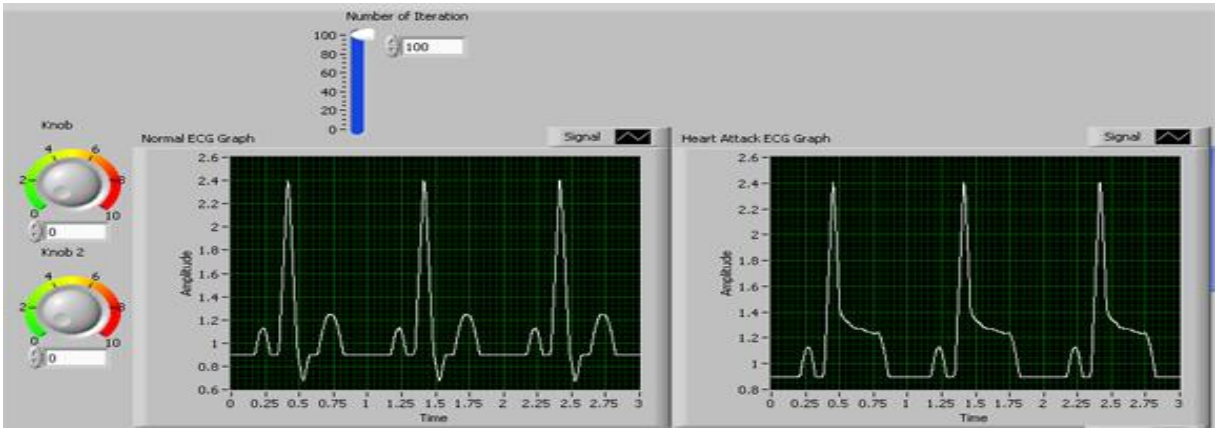

Figure 7: Normal ECG signal (on the right) and a heart attack signal (on the left) generated using LabView™

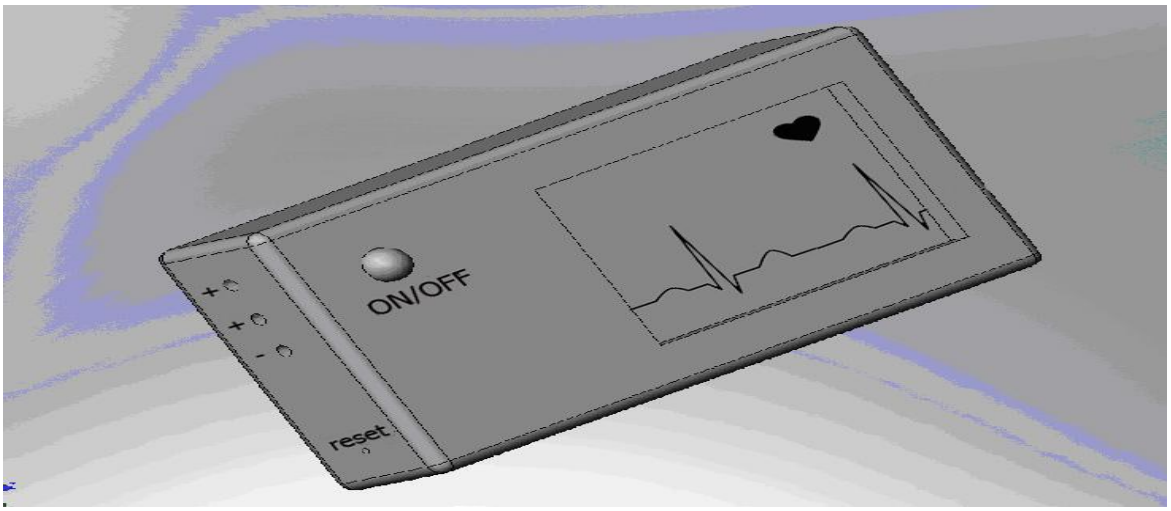

Figure 8: Physical design of the wireless ECG monitor system

The result of the wireless ECG project and the prototype was promising and valuable. It was a relatively simple system, which could detect abnormality of the ECG signals within reasonable timing after the onset of heart attack. However, abnormal electric potential changes of the heart occur after the heart muscle is substantially damaged and usually is not a gradual change and can occur as a neurological malware of the heart. In addition, there exist a high chance of false positive and false negative associated with this type of detection. Therefore, a more reliable method was required to detect heart muscle damages at an earlier stage. Hence, a real time biophotonic approach was pursued to measure the level of specific blood components (biomarkers) which could detect damages at an early stage.

2: BIOPHOTONICS APPROACH TO CTNI MEASUREMENT

2.1 Introduction

As mentioned in the previous section, a biophotonic approach was pursued in detecting early Myocardial Infarction (MI) and for this purpose biomarkers were studied. Figure 9 illustrates different cardiac biomarkers and their level in the circulation system versus time after an MI.

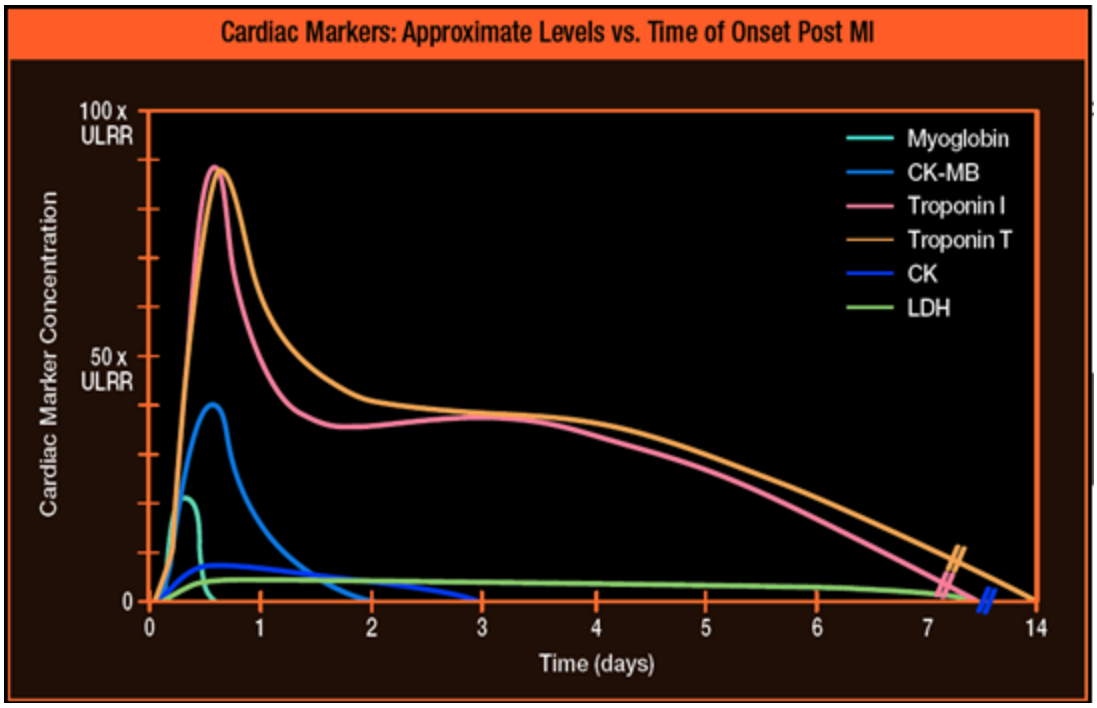

Figure 9: Approximate level of cardiac biomarkers after MI (Modified from [4])

According to a large number of studies, cTnI is the current "Gold Standard" test for diagnosis of MI. Compared to other cardiac biomarkers (i.e. CK-MB and Myoglobin), cTnI has superior sensitivity, higher specificity and, more ability to detect heart muscle damages [4].

Detectable level of cTnI is reached in 3-6 hours after a MI and will peak within 14 to 20 hours and return to normal after 5 to 7 days. The normal concentration of cTnI in serum is below

0.1 µg/l [5]. In MI patients, this level raises to as high as 100 to 300 µg/l, an increase of 1000 to 3000 folds. This significant increase in concentration along with specification of cTnI to heart muscles solves the problem of other cardiac biomarkers false positive for conditions unrelated to MI.

2.2 Background

Cardiac troponin I is part of the cardiac troponin complex, which was first discovered by Dr. Setsuro Ebashi. The troponin complex, a component of the heart muscle fibers is composed of three single-chain polypeptides, which are listed below [6]:

- Troponin-I (TnI) which prevents muscle contraction in the absence of calcium.
- Troponin-T (TnT) which connects troponin complex to tropomyosin.
- Troponin-C (TnC) which binds to calcium.

After onset of MI, due to lack of oxygen supply, cardiac muscle fibers begin to release their component into the bloodstream. Troponin, which is one of the components of the muscle fibres, is released into blood causing significant increase in concentration of cardiac troponin in peripheral circulation. Since troponin release takes place at a lower threshold of oxygen deficiency of the cardiac muscle cell than CK, troponin test is a more sensitive test.

Figure 10 presents the troponin complex before heart muscle damage, free troponin components after heart muscle damage and decomposition of the complex. The 3D structures of free (not in the complex) cTnI, cTnC and cTnT respectively are shown in Figure 11.

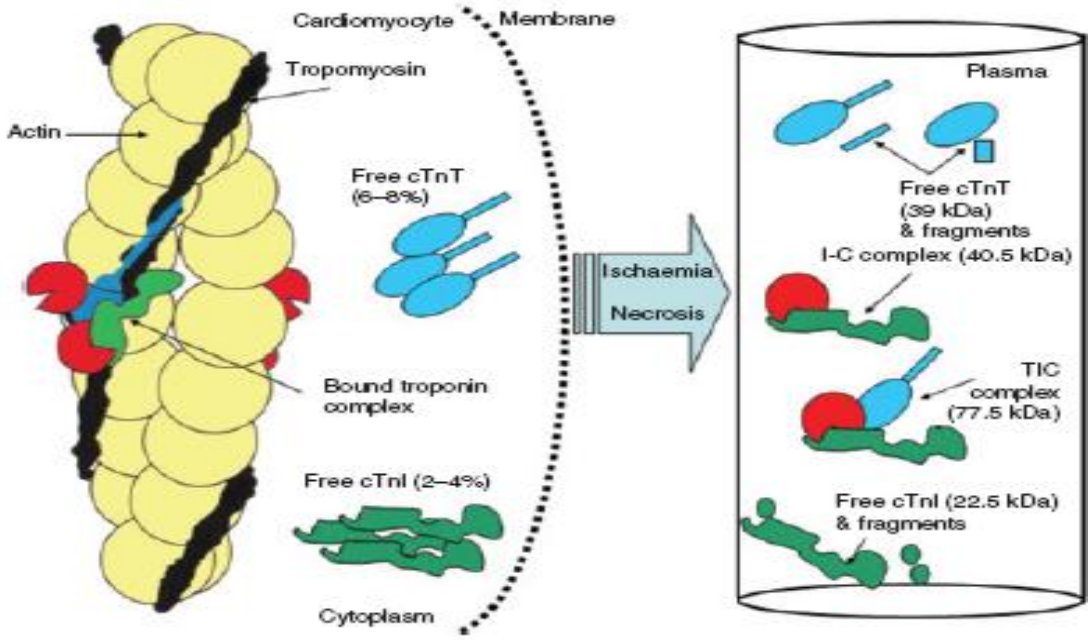

Figure 10: Troponin Complex Decomposition (Modified from [7])

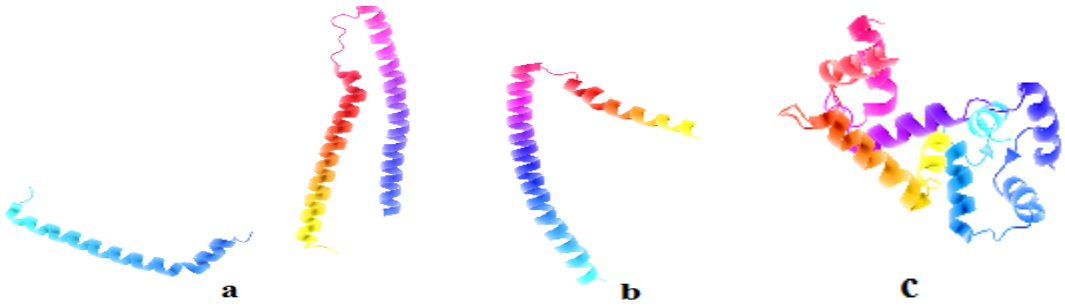

Figure 11: a. cTnI, b. cTnT and c. cTnT (Modified from [8])

2.2.1 cTnI vs. cTnT

Although there is a strong consensus of the clinical agreement between the result of the cTnI and cTnT test, some minor differences are apparent. The vast majority of studies support similar clinical utility between the two tests, but a few exceptions have been published [9]. At least one

recent paper concluded that using the recommended cut points for cTnT and cTnI, safe discharge was only achieved with patients tested using cTnI.

Another research showed that patients with inclusion body myositis had elevated cTnT with no elevation in cTnI in the absence of any indication of myocardial damage [10]. Therefore, it can be concluded that the potential probability of false-positives result for cTnT is higher. Also an exclusive patent has been issued for cTnT tests therefore most researches are done on cTnI.

2.2.2 Existing Solutions

Enzyme-Linked Immunosorbent Assay (ELISA) is a biochemical method used for measuring the concentration of a particular protein in a solution.

There are two main forms of the ELISA assay:

1) Direct ELISA, which uses monoclonal antibodies.
2) Indirect ELISA which uses a primary and secondary antibody.

The final step for both cases is to add a substrate to the solution. The substrate is then converted to a detectable form by enzymatic reaction for identification and quantification purposes [11].

The ELISA is one of the most rapid, sensitive and reliable troponin concentration measurement methods, which involves an enzyme (a protein that catalyzes a biochemical reaction), an antibody and an antigen (troponin). ELISA tests are widely utilized to detect substances that have antigenic properties, primarily proteins. ELISA detection of cTnI is based on an assay for the quantitative measurement of cTnI which uses four unique monoclonal antibodies directed against distinct antigenic determinants on the protein (Epitope). Three mouse monoclonal anti-cTnI antibodies are used for solid phase immobilization. The fourth antibody is

in the antibody enzyme (horseradish peroxidase) conjugate solution which is normally a secondary antibody that is conjugated to horseradish peroxidase (HRP) and cross reacts with the primary anti-cTnI antibody. The test sample is allowed to react simultaneously with the four antibodies, resulting in the troponin I molecules being sandwiched between the solid phase and enzyme-linked antibodies. After 90-minutes of incubation at room temperature, the wells are washed with water to remove unbound-labelled antibodies. A solution of tetramethylbenzidine (TMB) reagent is added and incubated for 20 minutes (to react with the enzyme, horseradish peroxidase), resulting in the development of an end product with blue color due to its aromatic structure. The color development is stopped with the addition of 1M hydrochloric acid (HCl) changing the color to yellow. The concentration of troponin I is directly proportional to the color intensity of the test sample. Absorbance is measured spectrophotometrically at 450 nm [12]. Figure 12 presents the test principle of Labmaster Troponin I ELISA test which is a two-step enzyme linked immunosorbent assay [13].

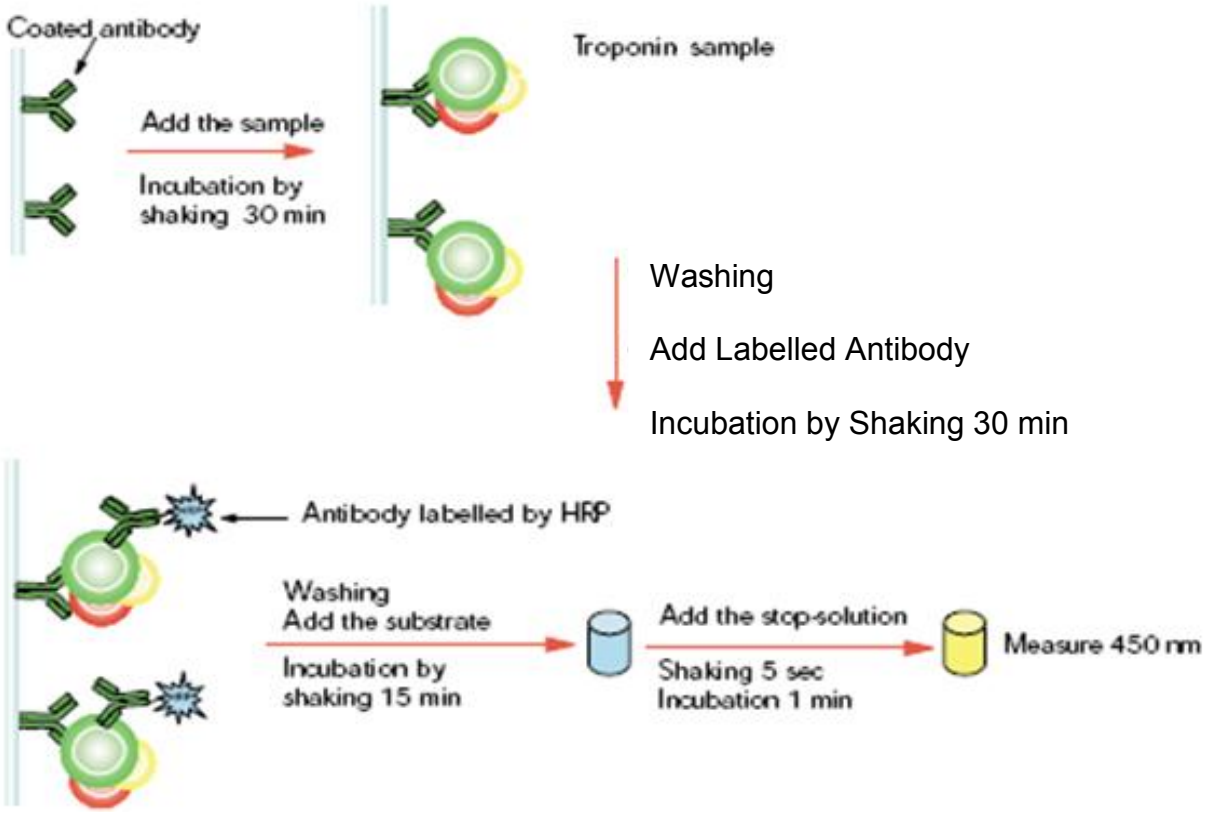

Figure 12: Labmaster Troponin I ELISA test principle (Modified from [13])

Since the HRP reaction for this specific ELISA kit has the highest absorption characteristic at 450 nm, absorption is measured at this wavelength. Result of a typical standard run with absorbency reading at 450 nm of troponin I versus concentration using ELISA method is shown in Figure 13. The standard curve shown in this figure is for the purpose of illustration only [12].

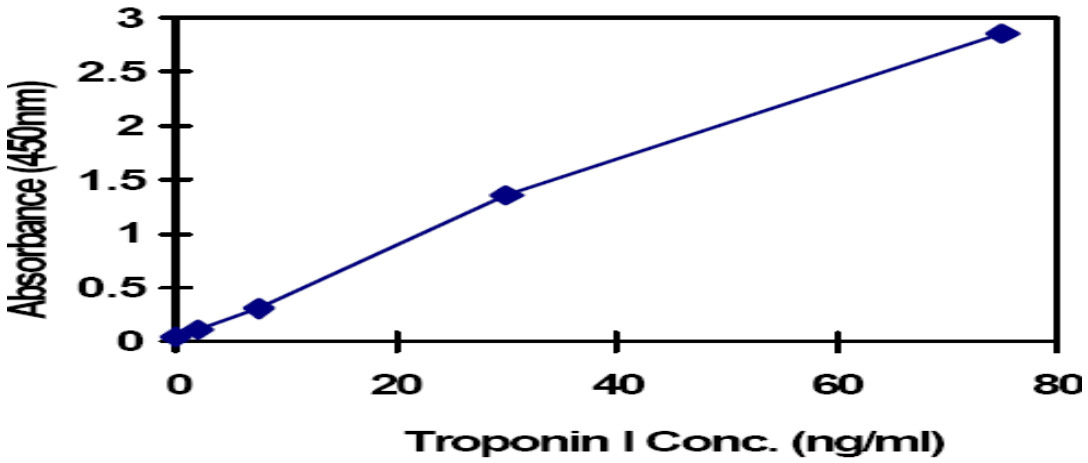

Figure 13: Standard Curve from Assay procedure (With permission from [13])

A list of available devices currently used to measure the concentration of Troponin I or T based on the proceeding concept are summarized in Table1.

Table 1: List of a number of existing Troponin measurement devices

Triage® Cardiac Panel
TROPT ®
Roche ® Cardiac Reader
VIDAS® TnI ULTRA
DPC Immulite cTnI
OCD Vitros ECi cTnI
Dade Dimension RxL cTnI
Beckman Access cTnI
Bayer Advia Centaur
Tosoh AIA 600 II cTnI
Abbott Architect cTnI
Roche Elecsys 2010 cTnT

2.3 Molecular Structure of cTnI

Some proteins may have fluorescence properties due to the presence of aromatic amino acids. The position of amino acids and tertiary structure of protein determines the protein's fluorescence characteristics. The three aromatic amino acids are:

- Tryptophan(W)
- Tyrosine(Y)
- Phenylalanine(F)

Human cTnI Amino Acid Sequence is shown in Figure 14.

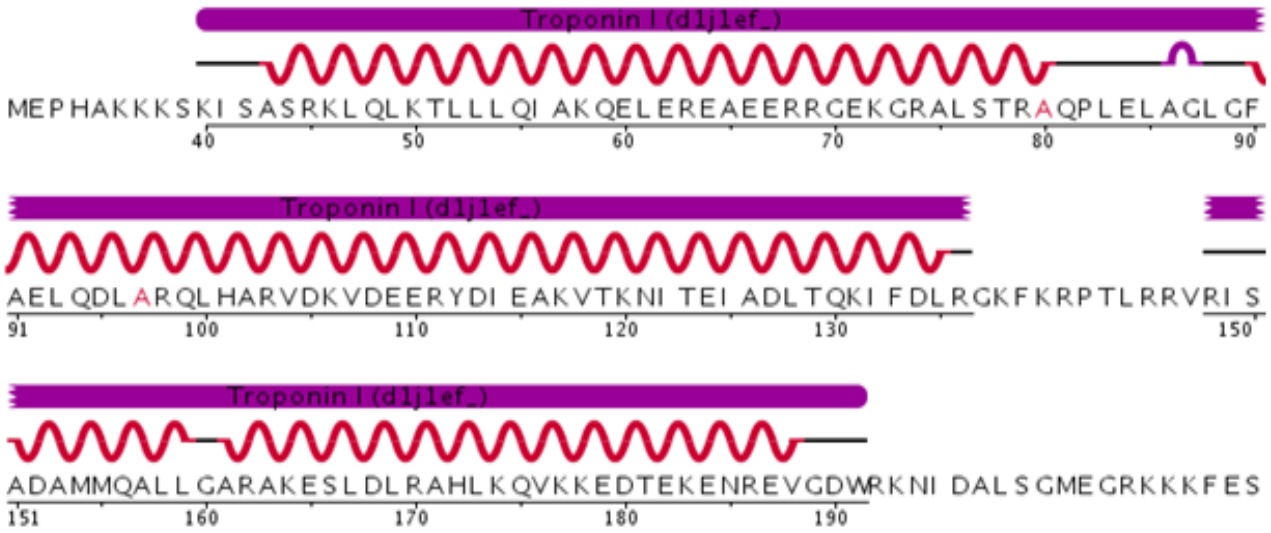

Figure 14: Human Cardiac Troponin I Amino Acid Sequence (Modified from [8])

Due to the presence of Tryptophan (W) at residue 191 (as shown in Figure 16), fluorescence characteristics can be expected from human cardiac troponin I.

Conjugated systems of fewer than eight conjugated double bonds absorb only in the UV region and are colorless to the human eye. With every double bond added, the system absorbs photons of longer wavelength (and lower energy). Table 2 presents the fluorescent excitation and emission wavelength of conjugated amino acids.

Table 2: Florescent profile of conjugated amino acids

Amino Acid	*Excitation Wavelength*	*Emission Wavelength*
Tryptophan	280 nm	348nm
Tyrosine	274 nm	303 nm
Phenylalanine	257 nm	282 nm

Many factors contribute to the florescence intensity and wavelength of proteins. For example Tryptophan residues buried in the hydrophobic core of proteins can have spectra which are shifted by 10 to 20 nm compared to a Tryptophan on the surface of the protein. Moreover Tryptophan fluorescence can be quenched by neighbouring protonated acidic groups such as Aspartic acid (D) or Glutamic acid (E).

2.4 Purpose of Biophotonics Measurement of cTnI

The main purpose of this project is to investigate the design of a possible heart attack detection system, which could detect heart muscle damage shortly after the onset of MI based on the increase of cTnI concentration in the bloodstream. In addition, this project allows for investigation on feasibility of the purposed system.

2.5 Florescence Spectroscopy Experiment

The experiment started with sample preparation of known concentrations of purified cTnI. The next step was to characterize the excitation and florescence wavelength of the protein to be

used as reference for future data acquired with the designed system. A PTI Quantamaster UV-Vis Spectrofluorometer was used to find the excitation and emission wavelength of cTnI.

2.5.1 Components Used for Fluorescence Spectroscopy Experiment

The following components were used to build an optical system for this project:

HBO 200 W Mercury Arc Lamp
First Surface Spherical Mirror
11 mm uncoated lens
1800 grooves/mm Newport Plane Ruled Reflection Grating
10 mm UV Quartz Fluorescence Cell

A SPM-002E Photon Controller Spectrometer with the spectral range of 200-1090 nm was used to detect florescence. SPM-002E is silicon CCD Spectrometers based on the 3648 pixel Toshiba TCD1304 CCD [14]. Also a Newport PowerMeter was used to measure the absorption characteristics of cTnI. Figure 15 presents a picture of these detection devices.

Figure 15 : Spectrometer and Power Meter

2.5.2 Fluorescence Spectroscopy Experiment setup

Figure 16 illustrates the optical set up designed for this project. The alignment of the components had to be changed and configured by adjusting the angle and distance of the components in order to spot the focus points created by each component.

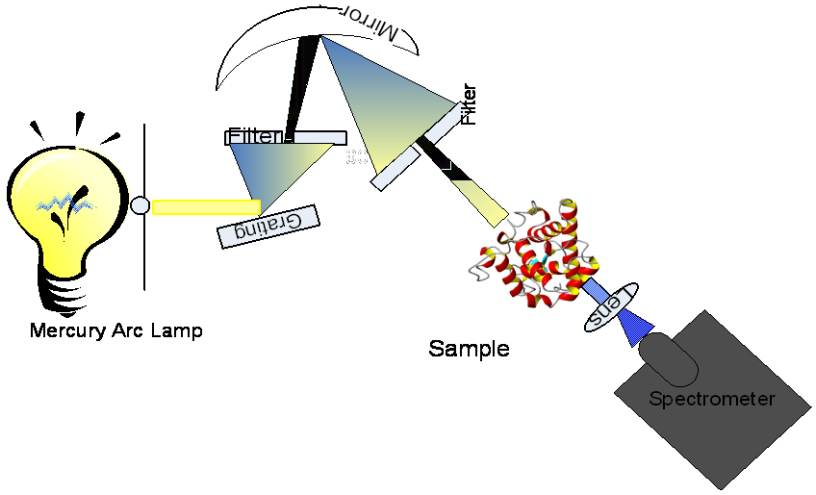

Figure 16: Optical Florescence Experimental Setup

In order to calibrate the spectrometer, an experiment was set up with four different food colours in order to observe the absorption at different colours by the UV light source.

The parts used for this experiment are mostly from salvage to reduce costs. However, these parts were sufficient to build a basic optical setup for demonstration. The intended future experimental setup requires a more complicated system design and components. Shorter UV specific optical cables should be used and Back-Thinned CCD spectrometer can be exploited instead of the silicon spectrometer. This spectrometer is based on the Hamamatsu S9840 back-thinned CCD technology which operates at a very high UV sensitivity (with quantum efficiency of 55% at 250 nm) and has a high dynamic range of 5200:1 [15]. In addition, the same configuration and spectrometer can be used for absorption and concentration change measurements. Moreover, instead of the diffraction grading setup, two optical filters (band-pass and band-reject) with 280

nm centre wavelength can be used to increase the efficiency of the overall system. Figure 21 presents the physical set up for the fluorescent experiments and Figure 17 illustrates the physical set up for the absorption measurements of the cTnI sample. The last lens in the optical setup serves as both a converging lens and band-reject filter at 280 nm since it absorbs UV light up to 300 nm range.

Figure 17: Physical set up for florescence

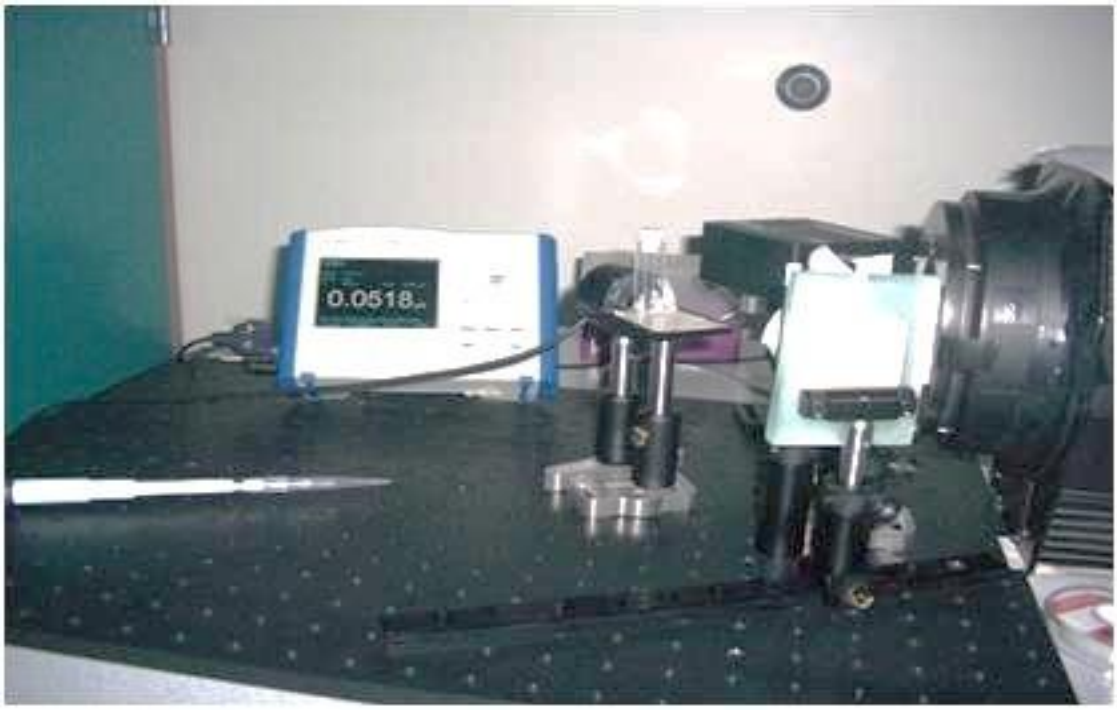

Figure 18: Physical set up for absorption

2.6 Fluorescence Spectroscopy Experiment Results

The expected mercury arc lamp UV-Vis emission spectrum is shown in Figure 19. The actual spectrum shows a small peak at 280 nm which is our desired wavelength as shown in Figure 20. The small peak was selected using the diffraction grating and the integration time was increased in order to be able to see the peak.

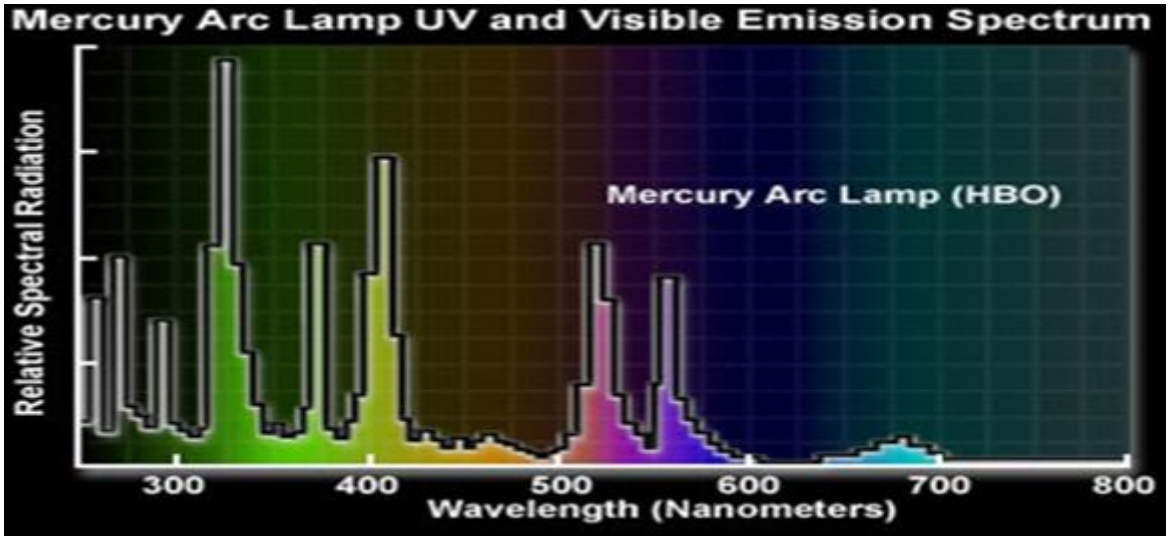

Figure 19: Mercury arc lamp expected spectrum (Modified from [16])

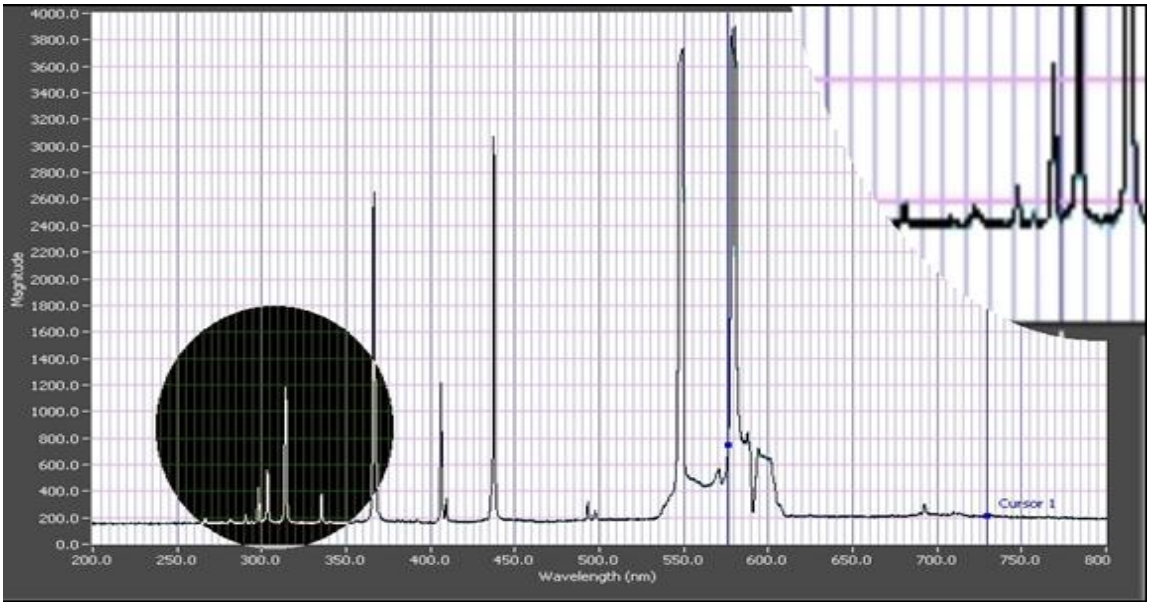

Figure 20: Mercury arc lamp spectrum from the spectrometer

Two paper filters were used in order to narrow the wavelength selection and reject the unrelated wavelengths. Figure 21 shows this effect.

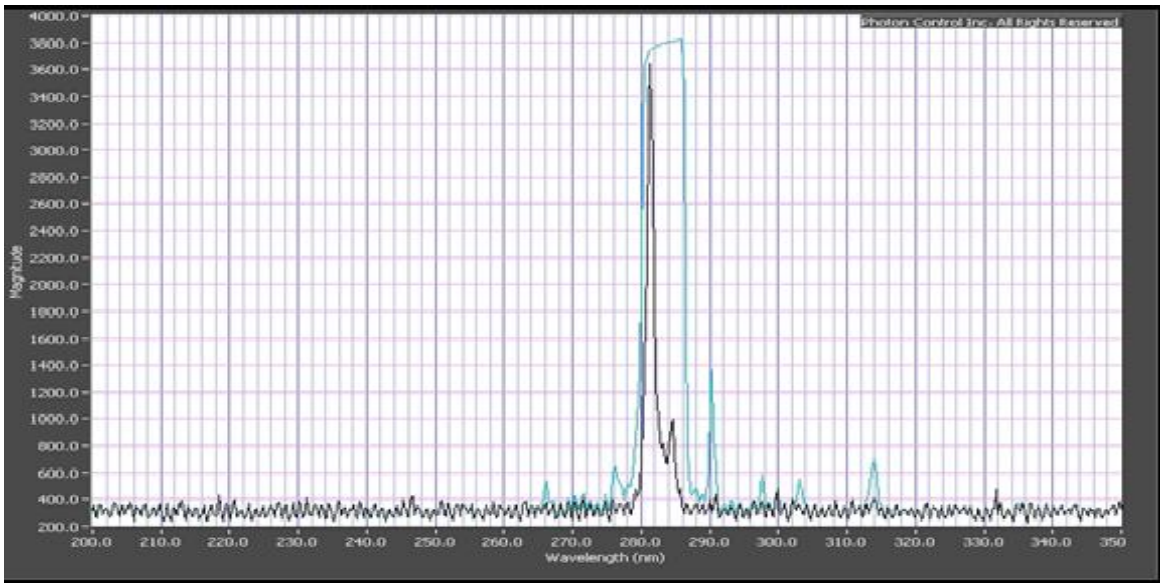

Figure 21: Effect of filtration

After many trials and adjustments in alignments and components, a small florescent signal were detected from the lens which is the white signal shown in Figure 22. Since the 280 nm wavelength was absorbed by glass, it was not necessary to use a filter to block the source.

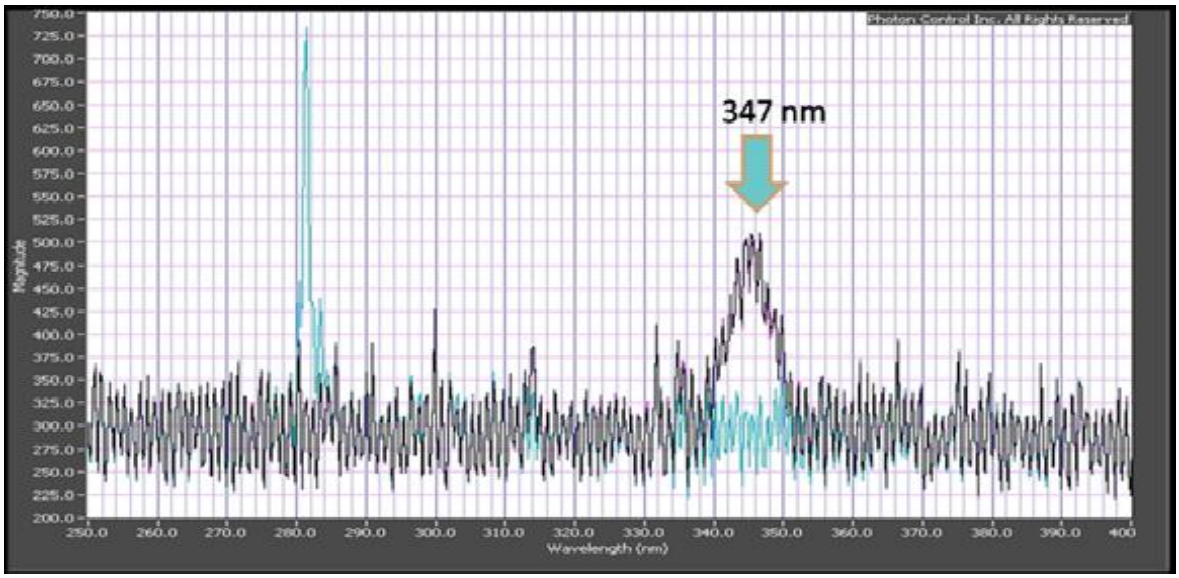

Figure 22: Fluorescence peak

In order to verify the experiment, after acquiring the 280 nm signal, the sample and the focusing lens were removed and the 280 nm signal was observed (the white signal shown in Figure 22). The green signal in Figure 23 is the previously detected 347 nm emitted from the sample.

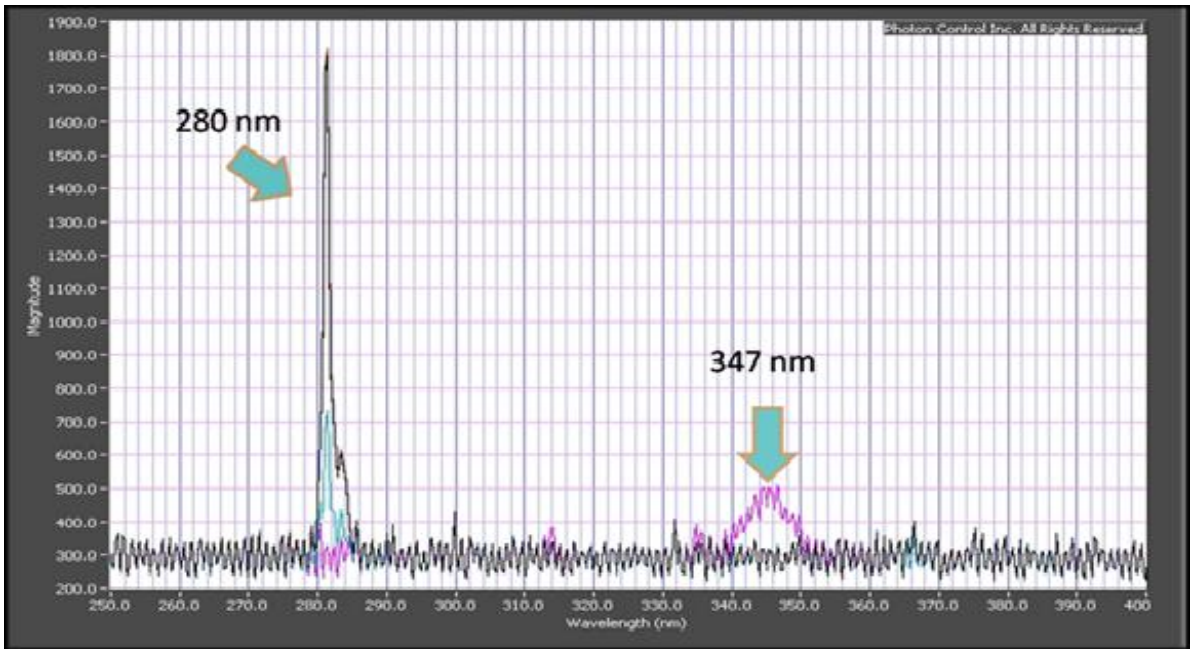

Figure 23: Source peak after the sample is removed

2.7 Discussion and Analysis

Using the result acquired from the PTI Quantamaster UV-Vis Spectrofluorometer of a complete scan through the cTnI sample, the excitation wavelength of the protein was acquired. As illustrated in Figure 24, the excitation wavelength of cTnI is 283 nm as expected from the existence of Tryptophan.

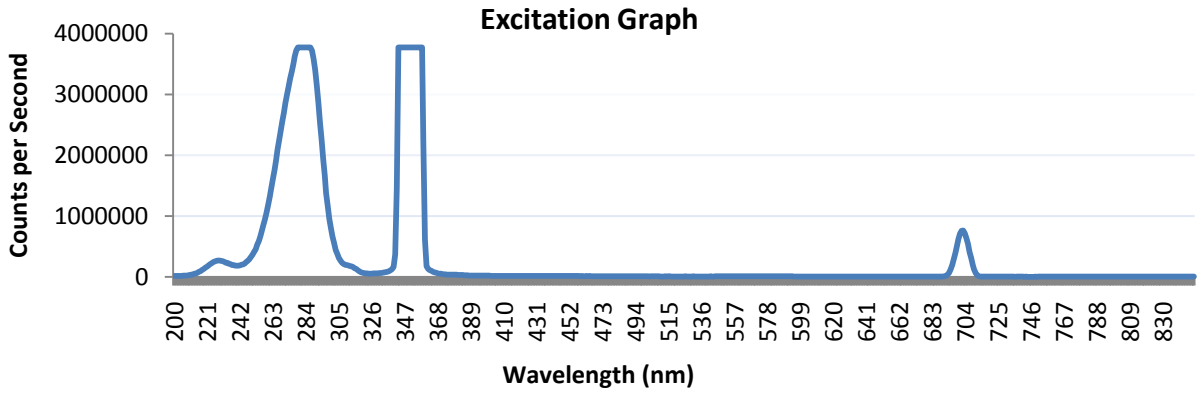

Figure 24: Scan through cTnI sample to find the excitation wavelength

The data graph of the emission of cTnI sample when excited at 280nm is shown in Figure 25. The peaks at higher frequencies than expected are artifacts due to PTI Quantamaster Spectrofluorometer performance since they have also appeared when scanning the negative control (water). The emission wavelength for different concentrations of cTnI in water happens at 347 nm as expected. The second peak which appears at higher wavelength is again caused by the device. Table 3 summarizes the peak values at various concentrations.

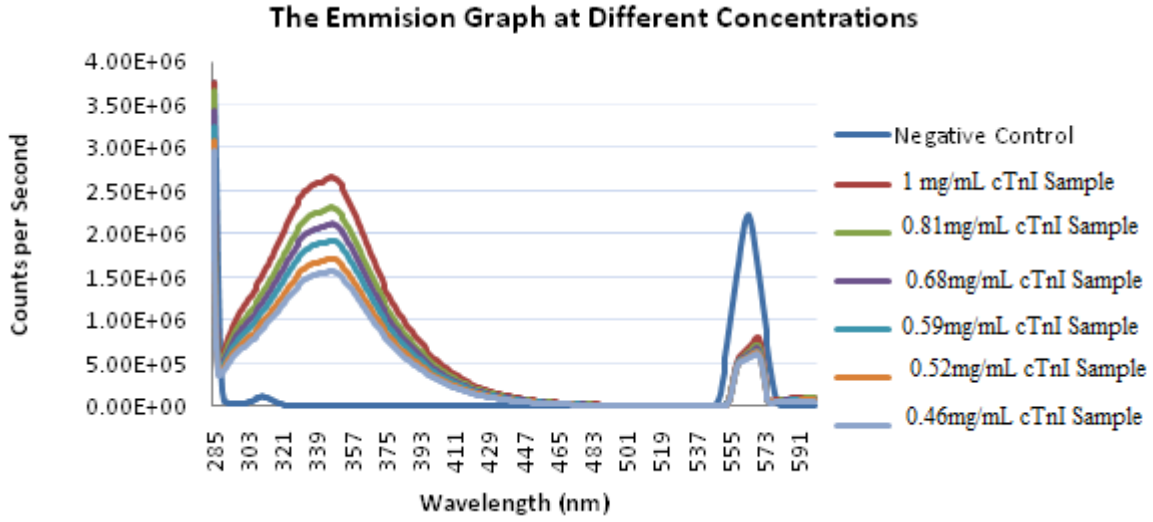

Figure 25: The emission wavelength at different concentrations when excited at 283nm

Table 2: The peak values at various concentrations of cTnI

Molarity(uM)	Peak Values
0	173657
18.96	2659630
21.44	2312060
24.73	2124130
28.03	1933120
33.39	1713940
41.22	1573370

The molecular weight of cTnI is 24,259 Da [8]. Table 4 summarizes the molarity of cTnI calculated using the molecular weight versus the absolute peak amplitude of intensity (where peak value at zero concentration is subtracted from the rest of the intensities). These values are plotted in Figure 26.

Table 3: The delta peak values at various molarities of cTnI

Molarity(uM)	Delta Peak Amplitude(count/sec)
0	0
18.96	1399713
21.44	1540283
24.73	1759463
28.03	1950473
33.39	2138403
41.22	3485973

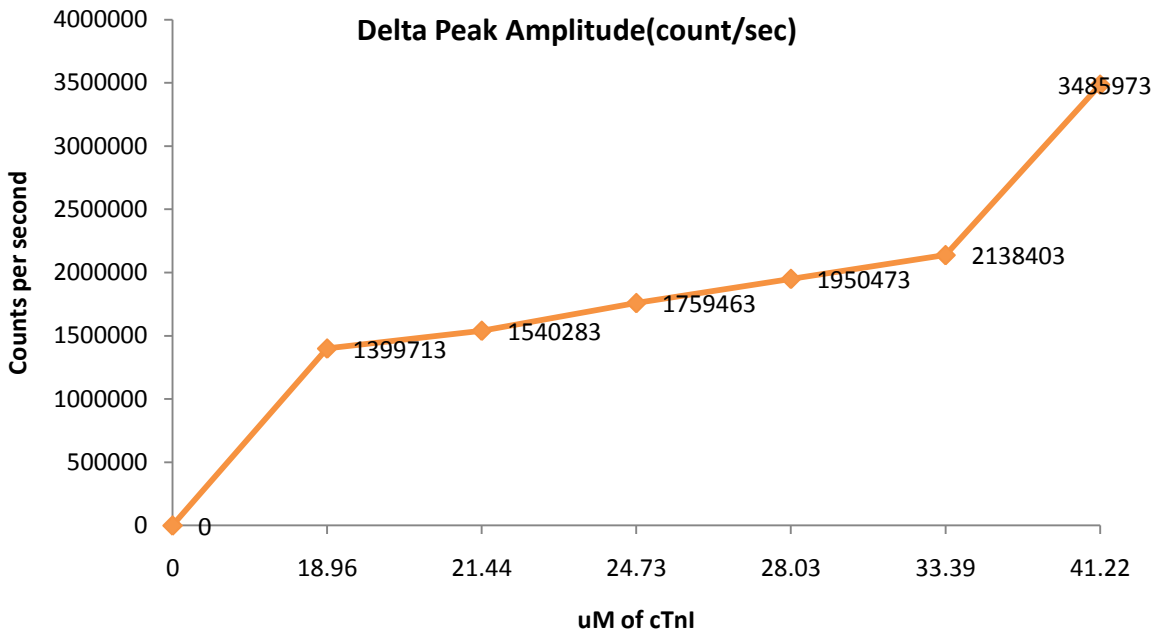

Figure 26: Absolute fluorescence intensity of various molarities of cTnI

In order to monitor the fluorescent behaviour of the protein with an increase in concentration, a linear regression analysis was performed (Figure 27). From the regression analysis output, the slope of the line is 48252 counts/μM, the y-intercept is 529833.6 counts and the coefficient of determination (R^2) is 0.95. This gives an indication of the fluorescence characteristic of this protein with respect to increase in concentration within the experimental and human error.

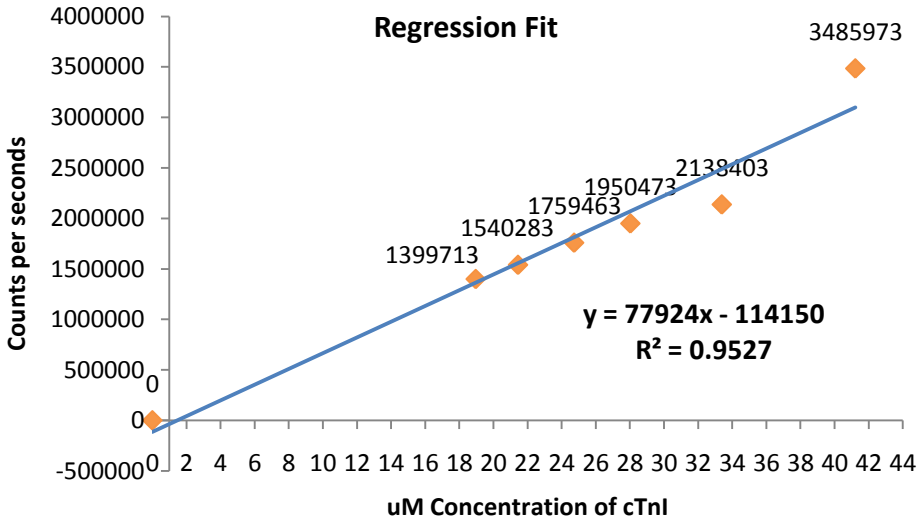

Figure 27: Linear Regression Graph

Using the absorption optical set up shown in Figure 18, the data presented in Table 5 was obtained at various concentrations.

Table 4: Absorption data

Power(uW)	Concentration(uM)
1165	0.00
519	76.26
488	83.19
428	91.51
402	101.68
342	114.391
314	130.732
272	152.521
245	183.025
197	228.781

The absorption data is plotted in Figure 28. It can be seen that the power versus concentration graph has a logarithmic behaviour. Therefore, we can conclude the absorption

characteristic is in agreement with the Beer-Lambert law as expected which is shown in the following equation.

$$A = -\log_{10}\left(\frac{I}{I_0}\right)$$

where I_0 and I are the intensity (power) of the incident light and that after the material, respectively [15].

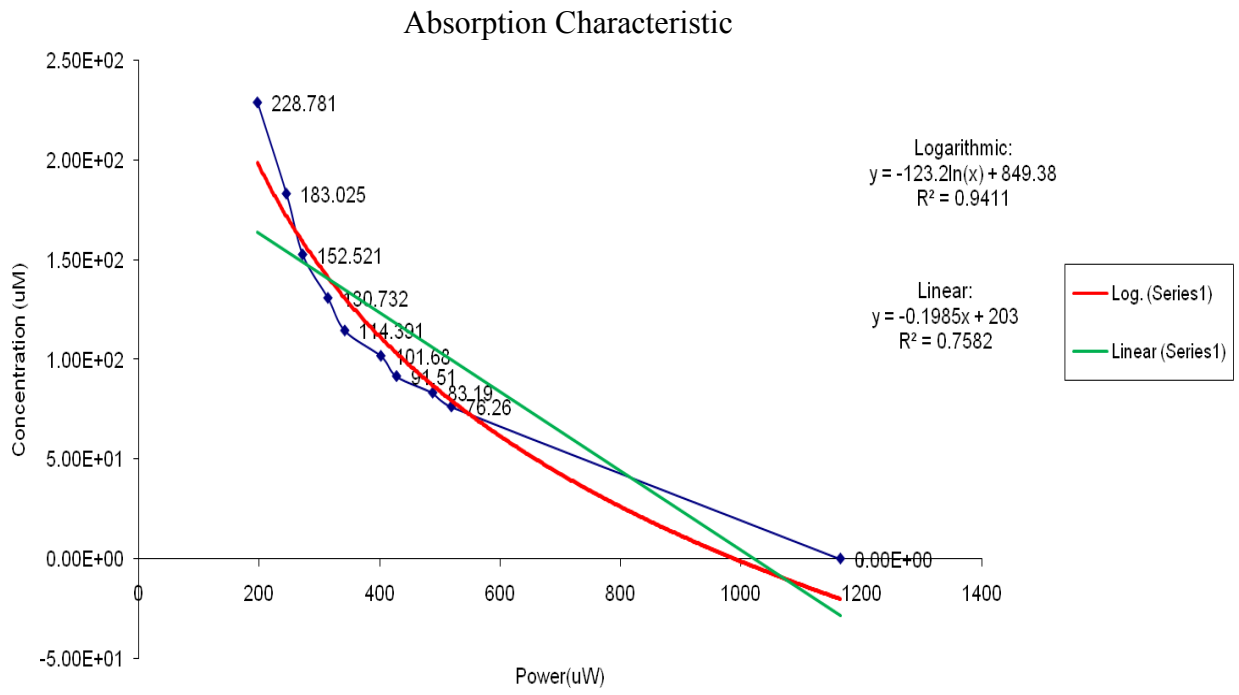

Figure 28: Absorption characteristic

2.8 Conclusion

In this chapter the fluorescence characteristics of cTnI protein was investigated and it was concluded that the data demonstrate a linear fit. Also the absorption characteristic of the same protein and four different food colours were investigated (for calibration purposes). The Beer-

Lambert law was confirmed to be valid for this protein. It should be noted that the concentration values used for this project were considerably higher than the normal concentrations in the human blood. The reproducibility of this project is very low due to lack of UV specific components such diffraction grating and lenses with higher efficiency at UV range also optical band pass filters for higher precision in wavelength selection. Most of the lights were absorbed by the components and the devices were not optimized for detecting very low florescent signals therefore the excitation beam was very weak.

In order to extract a unique characteristic of the protein from its emission/excitation profile and to be able to distinguish cTnI protein from other protein containing amino acids with conjugated properties, quantum effects should be considered. The high amount of noise and component limitations in emitted signal decreases the specificity of cTnI emission characteristics. Also detection of backscattered signal instead of the transmitted signal have higher amplitude and can be more reliable.

Therefore, the only anticipation which allows for further examination of this project is through the study of quantum changes in the cTnI protein after excitation and investigation of the Stokes shift and the quantum efficiency in measuring these small changes which leads to investigation on the Raman signature of the protein. At this stage combining Raman spectroscopy with Optical Coherent Tomography (OCT) seem to be promising since the detection of very small florescence signal amplitudes is very complicated and may not be possible using existing technologies and components.

3: RAMAN SPECTROSCOPY OF CARDIAC TROPONIN I

3.1 Introduction

Recently it has become very common to study physical and chemical changes occurring in tissues, cells and chromosomes using optical spectroscopy. Many different optical techniques are used, such as fluorescence, infrared spectroscopy, circular dichroism and Raman spectroscopy that are sensitive to the chemical composition and structure of biomedical species. Raman spectroscopy has the best fingerprinting capabilities of all other optical techniques aside from being easy to use and capable of collecting rapid spectral information. Unlike traditional optical techniques, Raman spectroscopy as an analytical tool makes it possible to combine the information about both the morphology and the chemical composition [16].

The weakness of fluorescence spectroscopy for the application of this research is due to the relative non-specificity of cTnI florescence signal in the blood, which is not easily distinguishable from other conjugated proteins. Therefore, we evaluated other possible spectroscopy methods for proteins. After an extensive literature review, Raman spectroscopy appeared to be the most promising method to distinguish cTnI from other proteins in the blood as every biological substance has a unique Raman signature.

3.1.1 Introduction to Cardiac Biomarkers

Even though the focus of our project is mainly on cTnI and partially on cTnT, in this section we briefly study other cardiac biomarkers to evaluate the future possibility of enhancing the reliability and sensitivity of the system. Table 6 presents normal concentration of cardiac biomarkers in the blood before heart attack and the elevated concentration of these cardiac biomarkers after a Myocardial Infarction (MI).

Table 5: Cardiac Biomarkers Concentration in the Blood pre and post MI [17]

Parameter	Control Subjects	AMI Patients
AST(mg/dl)	23±5.2	35±10.4
LDH(IU/L)	300±35	795±37.8
CK(IU/L)	73±15.6	126±26.5
CK-MB(IU/L)	12.5±2.8	97±7.8
Troponin T(ng/ml)	0.021±0.005	1.97±0.14
Troponin I(ng/ml)	0.32±0.05	3.17±1.1
CRP(mg/dl)	0.58±0.03	1.98±0.19
BNP(Pg/ml)	56±11	230±25.3

3.2 Raman Spectroscopy

Raman spectroscopy uses electromagnetic radiation at a specific wavelength to measure the energy exchange. Furthermore, as water is a weak scaterrer, this technique does not suffer from water interference and can therefore be used on biofluids and even *in vivo* measurements. [18] In addition, the Raman response of biological substances is a more specific type of measurement compared to fluorescence signal.

Dr C.V. Raman first discovered the method of Raman Spectroscopy in 1928 but only recently this method is being used as an analytical tool in many applications such as biology and chemistry. Due to the development of many industrial and research Raman spectrometers, this method is now relatively easy to carry out. One of the most important advantages of this method is its sensitivity and the high level of information that can be extracted from samples under study from the high level of information carried by their Raman signal. Moreover, this method is relatively non-destructive and has minimal water interference, which makes it a very good candidate as analytical tool for *in-vivo* protein measurement.

The proceeding section summarizes the progress of Raman spectroscopy of cTnI and cTnT project, which has been conducted at both SFU Molecular Cardiac Physiology Group lab and Grant Group lab at UBC. The objective of the research is to obtain Raman signature of cardiac biomarkers, Cardiac Troponin I (cTnI) and Cardiac Troponin T (cTnT) and characterize the resulting spectra. These proteins were studied because of their specificity to Myocardial Infarction (MI) and the concentration correlation with onset of heart attack. After finding the spectra, we create a model for concentration increase of these proteins. The ultimate goal, which can be extracted from the proceeding experiment, is to determine the concentration of cTnI or cTnT in the blood and *in vivo* by taking measurements from the blood vessels in the eye.

3.2.1 Background Information and Literature Review

After extensive literature review, we found several publications based on Raman spectroscopy analysis of various analytes. In one of the papers by Julia W. Evans *et al*, the concentrations of multiple analytes were simultaneously measured in whole human blood with clinical accuracy, without sample processing, using near-infrared Raman spectroscopy [18]. Spectra were acquired with an instrument employing non imaging optics, designed using Monte Carlo simulations of the influence of light-scattering–absorbing blood cells on the excitation and emission of Raman light in turbid medium. Raman spectra were collected from the whole blood drawn from 31 individuals. Quantitative predictions of glucose, urea, total protein, albumin, triglycerides, hematocrit, and hemoglobin were made by means of Partial Least-Squares (PLS) analysis with clinically relevant precision (R^2 values of 0.93). The similarity of the features of the PLS calibration spectra to those of the respective analyte spectra illustrates that the predictions are based on molecular information carried by the Raman light. This demonstrates

the feasibility of using Raman spectroscopy for quantitative measurements of biomolecular contents in highly light-scattering and absorbing media [18]. Figure 29 presents Raman spectra of 31 whole blood samples after polynomial background subtraction.

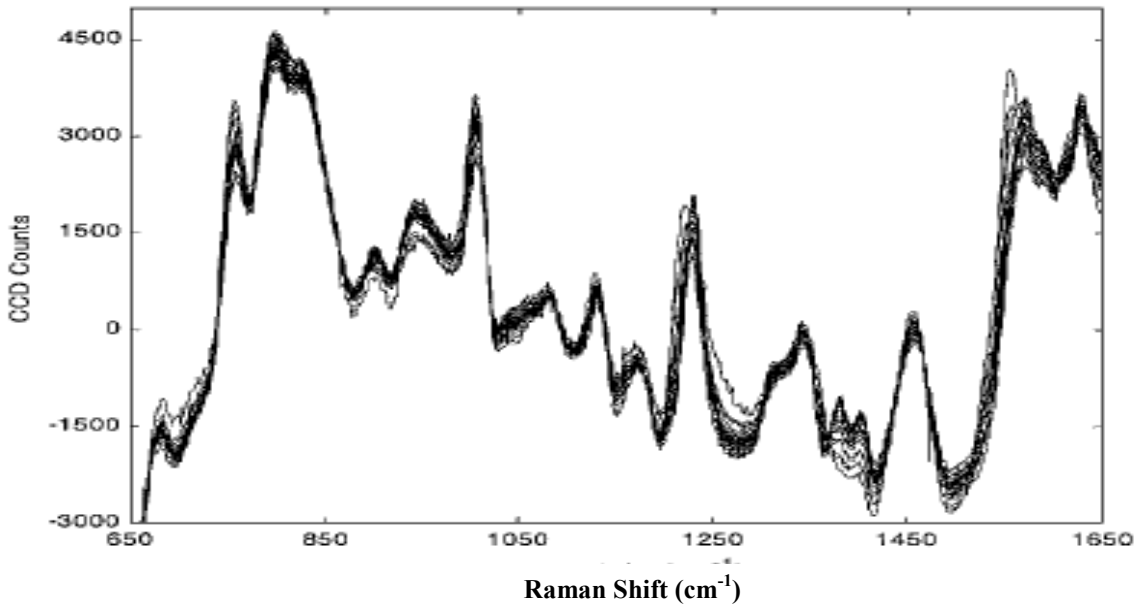

Figure 29: Raman spectra of 31 whole blood samples after polynomial background subtraction [19]

In order to replicate this result an experiment was conducted on mouse blood to find its Raman spectra. The specifications of the Raman Spectrometer instrument used for this experiment are as follows: wavelength is 785nm and the full laser power is 360mW. For this particular measurement, the integration time is 5 seconds. After removing the background, wavelet transform and extracting a portion of the wavelength, the result from the mouse blood did not have any extractable information due to the excessive noise caused by various components in the blood. Therefore, it was concluded that without completely characterizing the protein conducting experiment in the blood is not possible with the available technology.

Table 7 presents the predictions of analytes concentration in the blood acquired using Raman spectroscopy by Enejder *et al*. As shown in the table, Raman spectroscopy was used to measure the blood signature and the concentration of different analytes was estimated within physiological range. Consequently, these numbers are compared to the actual physiological range and the result was within the expected numbers.

Table 7: Analyte prediction from blood Raman spectroscopy (Modified from [19])

Analyte	Physio-logical Range
Glucose (mg/dL)	45–180
Urea (mg/dL)	17–50
Cholesterol (mg/dL)	150–250
Triglycerides (mg/dL)	10–190
Total Protein (g/dL)	6–8.3
Albumin (g/dL)	3.2–4.5
Hemoglobin (g/dL)	14–17.5
Hematocrit (%)	35.9–50.4
Bilirubin	0.1–1.2

Furthermore, we studied a patent on Raman spectroscopy in the human eye [20]. Even though the patent was intended for Raman spectroscopy measurement of blood glucose for diabetic people, it provides practical information regarding the steps that have been taken toward the use of this method for diagnosis. This invention provides methods for the use of Raman spectroscopy to non-invasively detect molecular characteristics of the constituents of the aqueous humor, vitreous humor, lens or retina. The method involves the steps of introducing light into the eye of the subject using laser, collecting Raman spectra onto the detector and analysing the detected spectra to identify molecular changes. The non invasive method provided by this invention makes use of techniques and equipments that enable detection of Raman Spectra with light intensities that fall within acceptable safety standards [20].

Our intended future approach would be similar to the mentioned system with the difference in the collection site being the area in the back of the retina close to the optical nerve in order to have direct access to concentrated blood vessels portion in the eye. For the testing purposes, we can also integrate the concepts from confocal microscopy in order to get signal only from regions of interest (where the laser is focused on a blood vessel in the retina). The conceptual design will be presented in Chapter 4.

The experimental plan was to identify the spectral peaks of wild type non-phosphorylated cTnI and cTnT in a buffer and later evaluate the possibility of identifying these peaks in the presence of noise by adding substances such as Bovine Serum Albumin (BSA) to the solution to make the situation closer to blood. The costume buffer was prepared based on I.M. Vlasova *et al* publication [21]. The details of the sample preparation are presented in Appendix I.

3.3 Spectral Result of Raman Spectroscopy Measurement of cTnI

In order to investigate the possibility of cTnI detection using Raman spectroscopy we designed and performed two experiments with different Raman Spectroscopes. For the first experiment, we used a commercialized SpectraCode RP-1 Portable Raman Spectrometer at SFU Physics Department. The result of this experiment is presented in Appendix II. This section presents various results from the second set of experiments, which was conducted at UBC Grant Groups Lab. The further measurements on several iterations of different concentrations of cTnI, cTnT and BSA in buffer are shown in the following figures. The apparatus setting is as follows: wavelength was 785 nm and the full laser power was 350mW. Figures 30 and 31 present the raw cTnI spectra in costume made buffer we prepared and in the BSA.

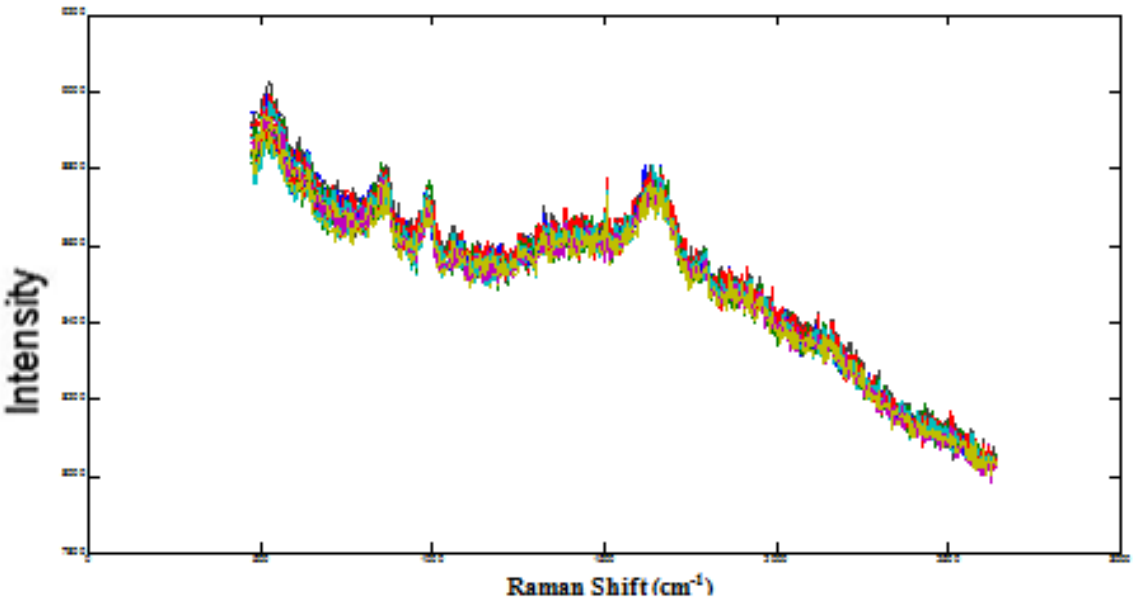

Figure 30: 10 mg/mL BSA in Buffer Sample Raman Signal

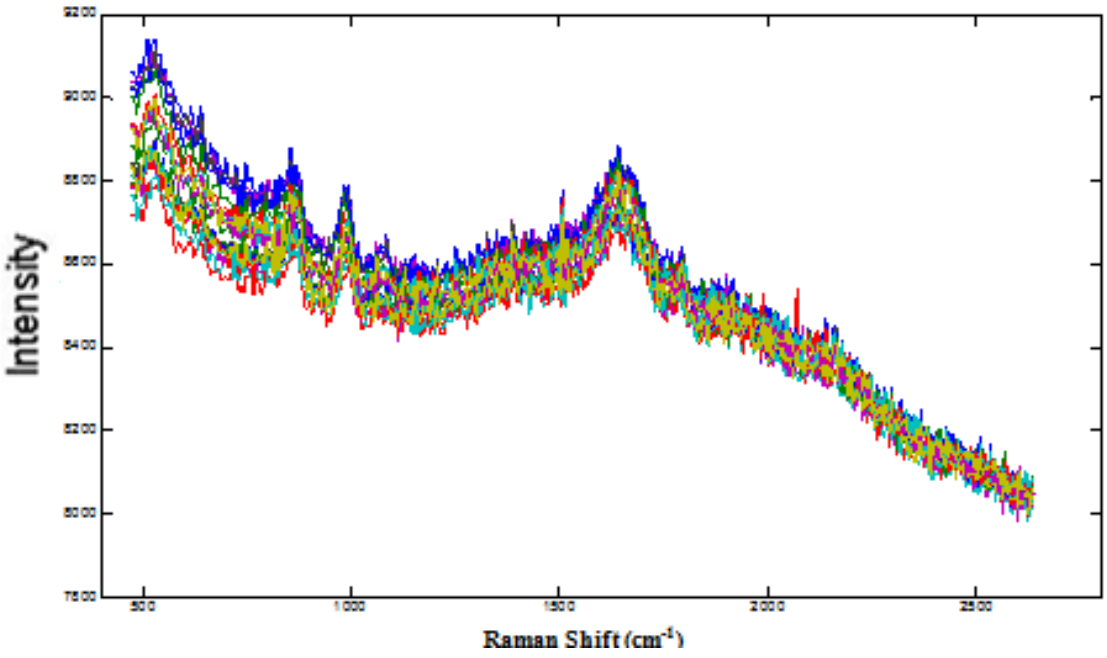

Figure 31: 0.49 mg/mL cTnI in Buffer Sample Raman Signal

Figures 32-36 are the processed spectra of the samples. In these figures, the spectrum of 10 trials for each concentration is averaged and the background noise is subtracted from the signal. As mentioned in previous sections with respect to sensitivity and specificity cTnT possess

similar characteristics to cTnI, therefore we acquired spectrum form this protein as well. The significance of analyzing cTnT in both the costume made buffer and BSA is to get insight on the differences between cTnI and cTnT and possibly investigate advantages of cTnT over cTnI for our purposes.

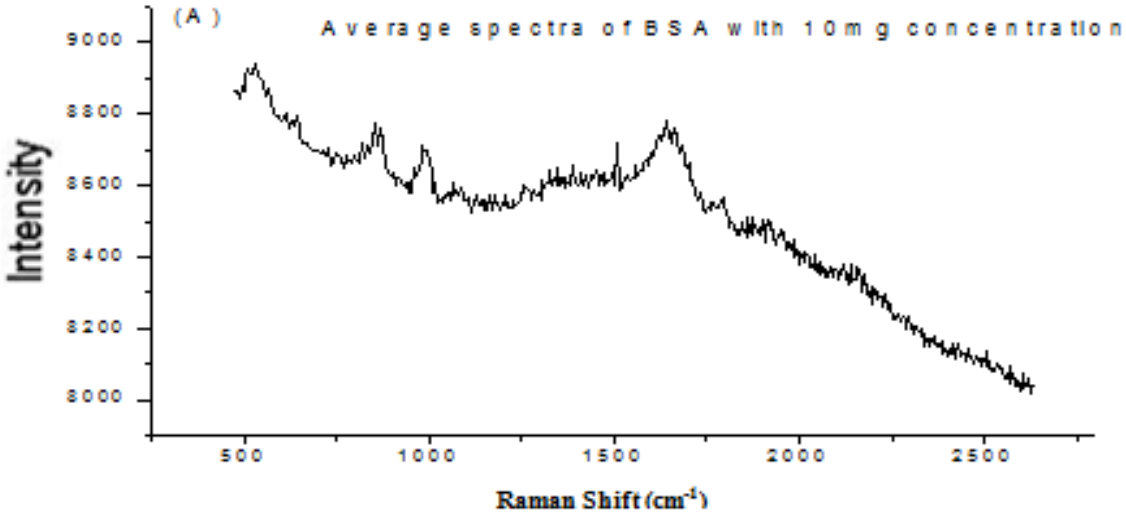

Figure 32: 10 mg/mL cTnI in Buffer Sample Raman Averaged

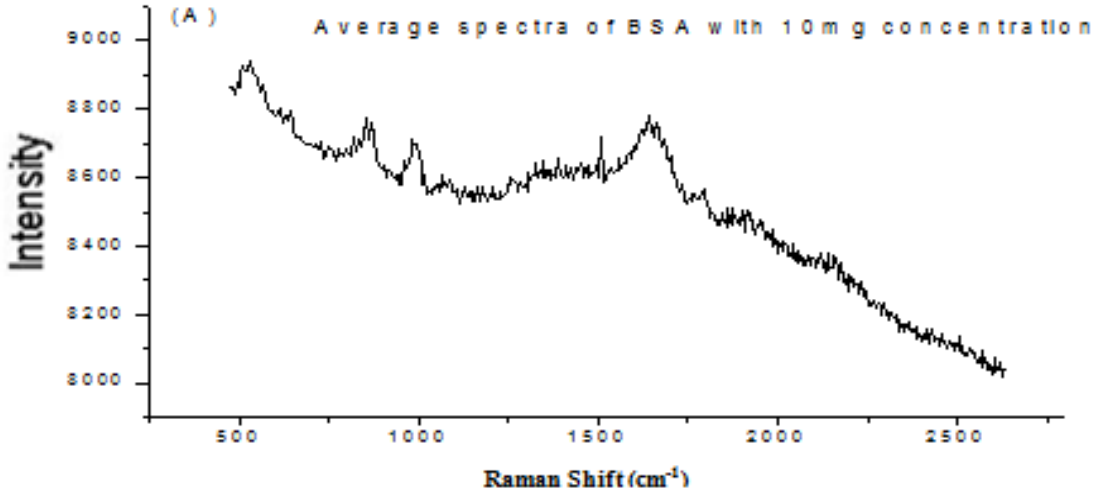

Figure 33: 0.49 mg/mL cTnI in Buffer Sample Raman Averaged

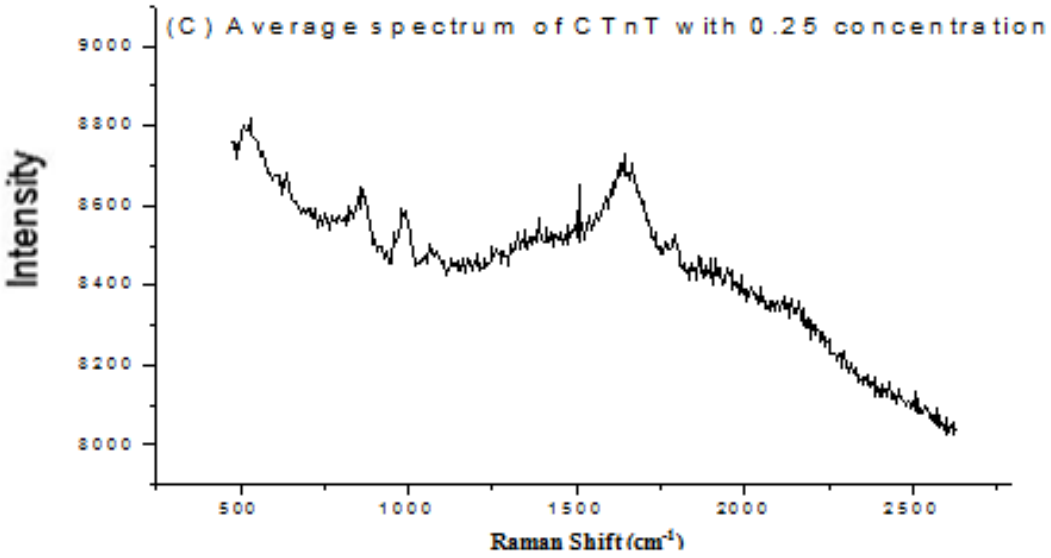

Figure 34: 0.25 mg/mL cTnT in Buffer Sample Raman Averaged

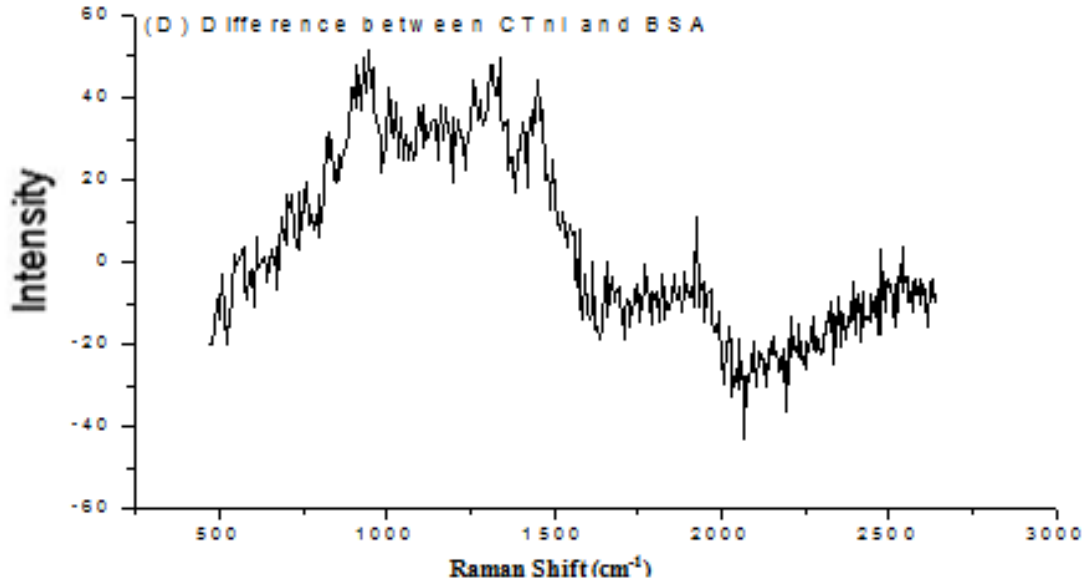

Figure 35: Difference between BSA and cTnI Raman signals

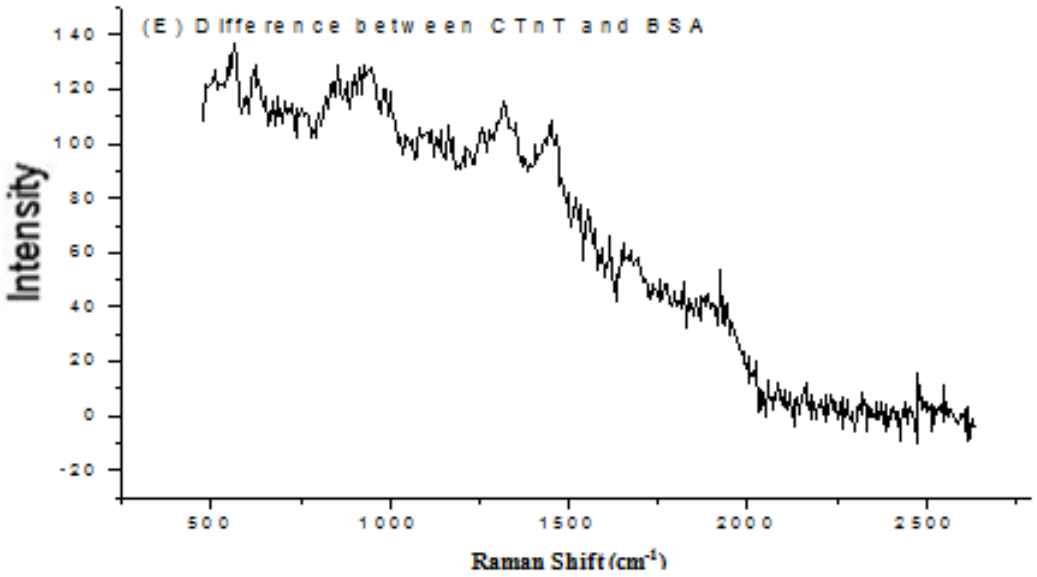

Figure 36: Difference Between cTnT and Buffer Raman Signal

Limited by the sensitivity and ratio of signal-to-noise (SNR) of current Raman instrument, the difference signal carries a large noise ratio. Although slight difference amplitude in some regions of the signal is observed, it is difficult to draw a conclusion to find the essential difference. Further investigation should be carried with the combination of the latest Raman instrument and chemometrics methods, which can greatly improve the SNR of Raman signal and make the difference more revealing. The new strategy will make the relationship between Raman spectral difference and cTnI absorption more clear and convincing.

In the next set of experiments, water is substituted from the solution to decrease the noise level. cTnT forms different configurations after it is released into the blood stream which makes the concentration of a single isomer of the protein even lower. Raman is sensitive to each isomer so when the number of isomer increases the concentration of each isomer is decreased therefore the intensity of the Raman signal is decreased for the highest concentration isomer. For this reason, further investigation of cTnI for our purpose was not necessary.

Figure 36 to Figure 41 present the raw and analyzed spectra for cTnI samples in water acquired at different laser power and integration time. The experiments are all performed using an industrial Raman spectrometer at UBC Grant Group Laboratory. The full laser power 140mW and the half laser power is 70mW. The analyzed data in the following graphs present the subtracted, averaged, and de-noised version of the raw cTnI spectra. Moreover, wavelet transform analysis has been performed on the results for easier distinction between the peaks of interest.

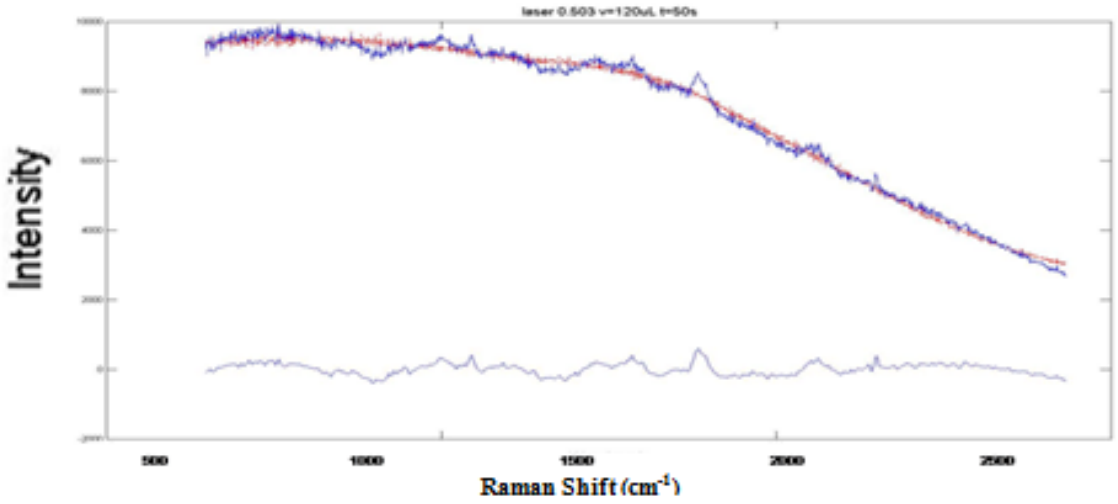

Figure 37: Half laser power and 50s Integration time cTnI Raman signal analyzed using wavelet transform

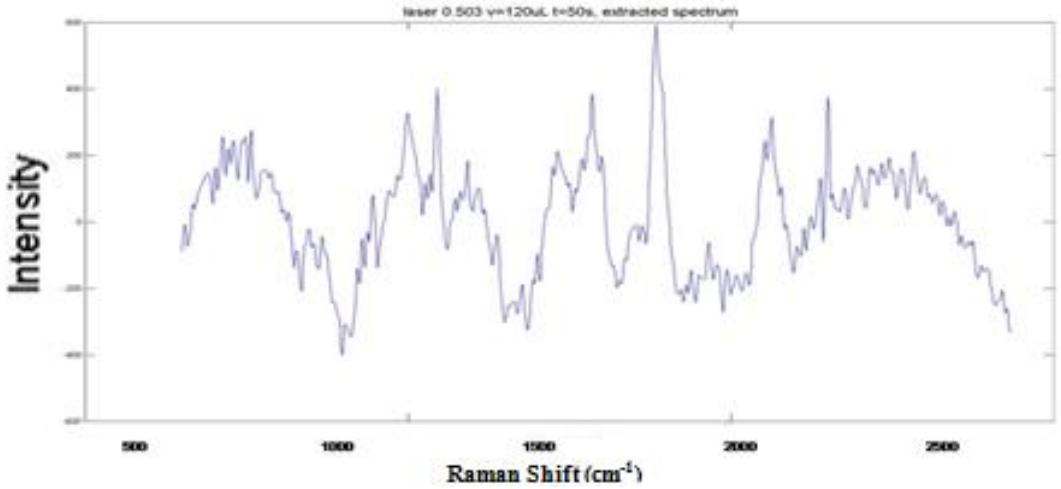

Figure 38: Half laser and 50 seconds Raman signal graph zoomed

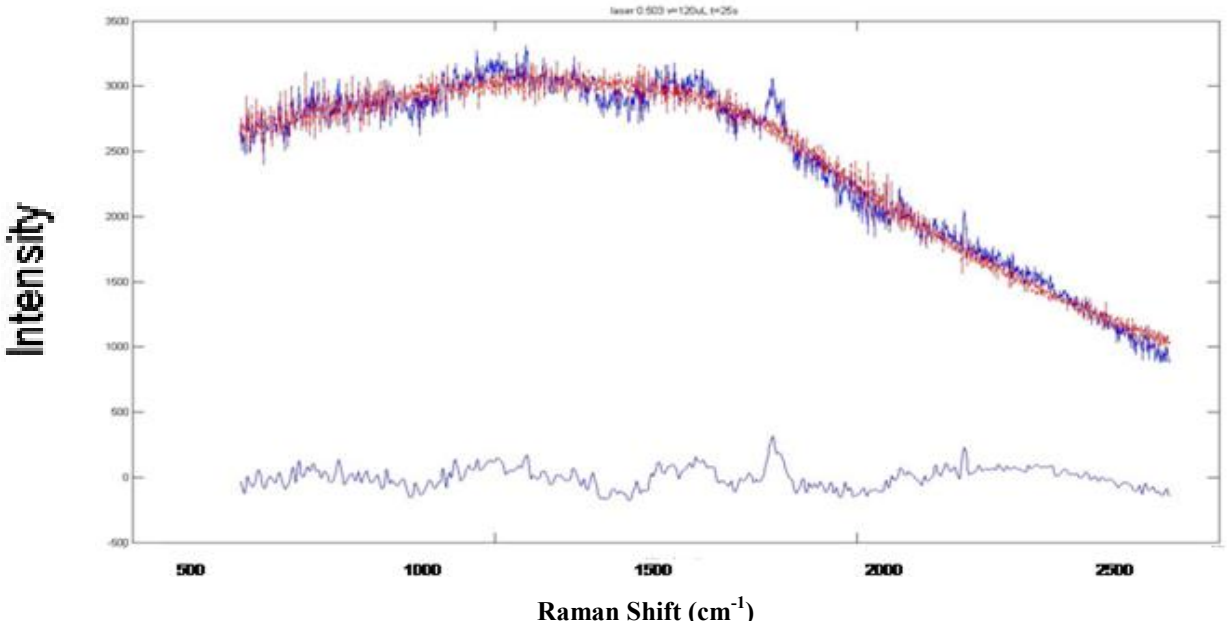

Figure 39: Half laser power and 25s Integration time cTnI Raman signal analyzed using wavelet transform

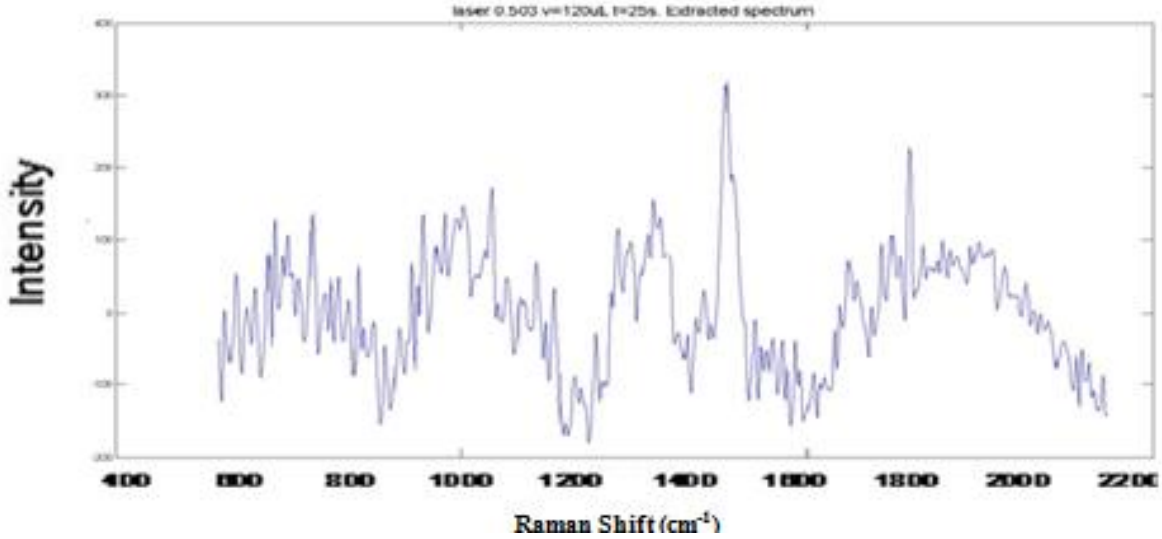

Figure 40: Half laser and 25 seconds Raman signal graph zoomed

As it can be noted from Figure 38 and 40, as the integration time is decreased, the signal-to-noise is also decreased.

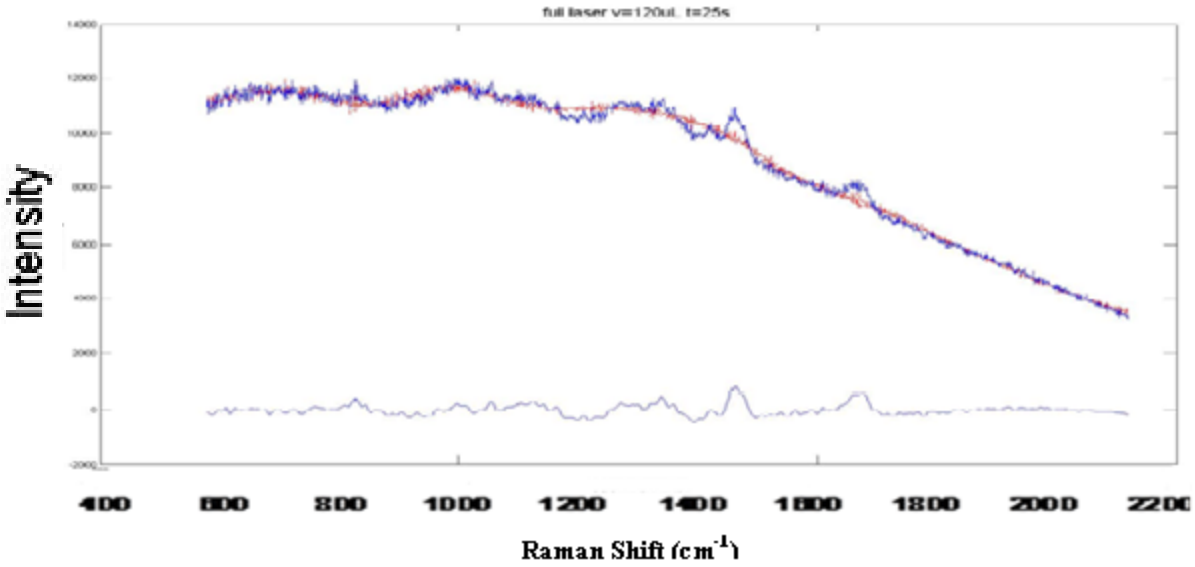

Figure 41: Full laser power and 25s Integration time cTnI Raman signal analyzed using wavelet transform

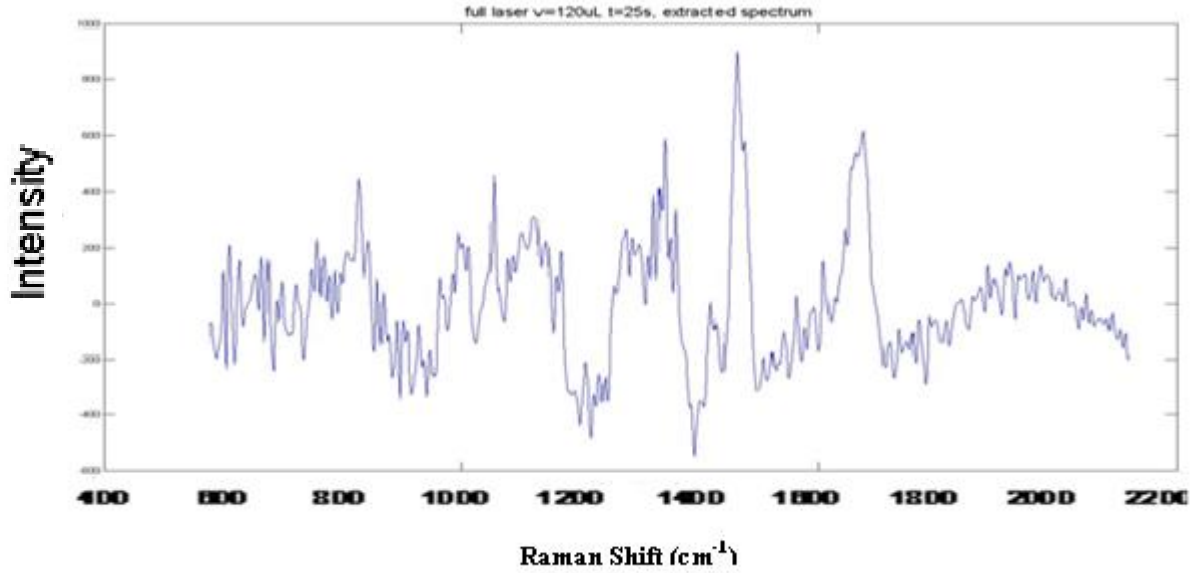

Figure 42: Full laser and 25 seconds Raman signal graph zoomed

By comparing Figures 40 with Figure 42, the effect of laser power on signal to noise ratio is evident since when the laser power increases the noise level in the spectra decreases. Also from the above spectra we can conclude that despite the low intensity of the signal, by characterizing the spectra as the concentration of the protein increases, cTnI can be measured in the plasma or blood. These results motive continuation of this research path to compare normal

and Myocardial Infarction (MI) mouse plasma and perform the above test to identify the differences in the Raman signal peak.

After finding the Raman signature of cTnI, the next step was to determine whether the signal intensity of the protein changes as the concentration is changed. The first set of experiments was conducted with fresh made (new) cTnI. The illustration of the effect of concentration change in new cTnI spectrums are presented in Figure 43. Figure 44 presents each concentration of old cTnI (made more than 1 year ago) separately when water spectrum is subtracted from the signal. The setting for the following experiments are as followed: laser power is 70 mW and integration time is 50 seconds

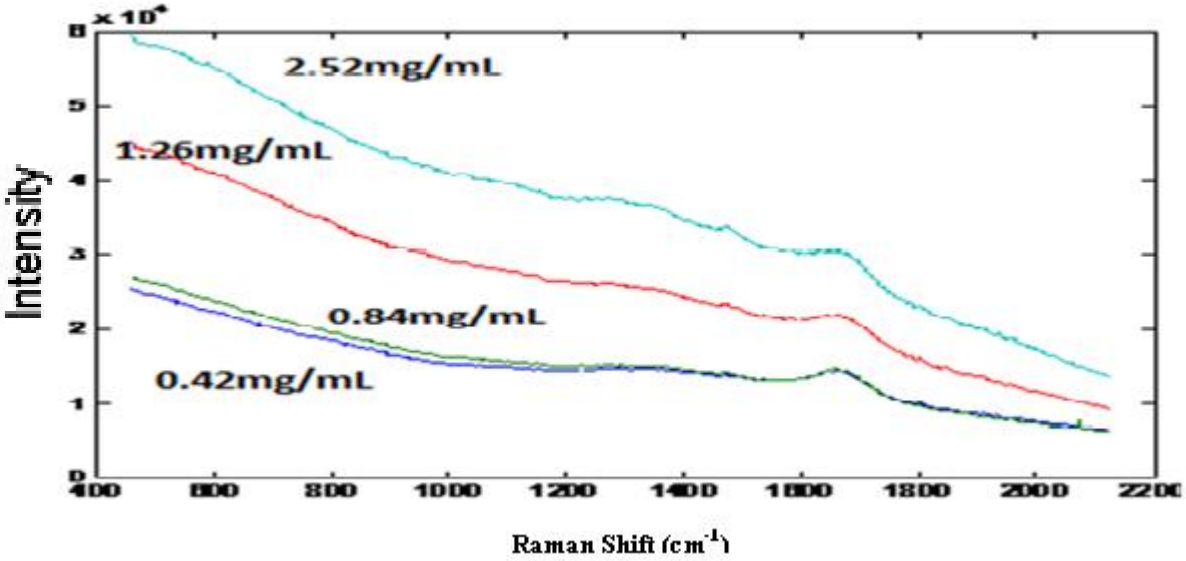

Figure 43: New cTnI Raman intensity for change in concentration

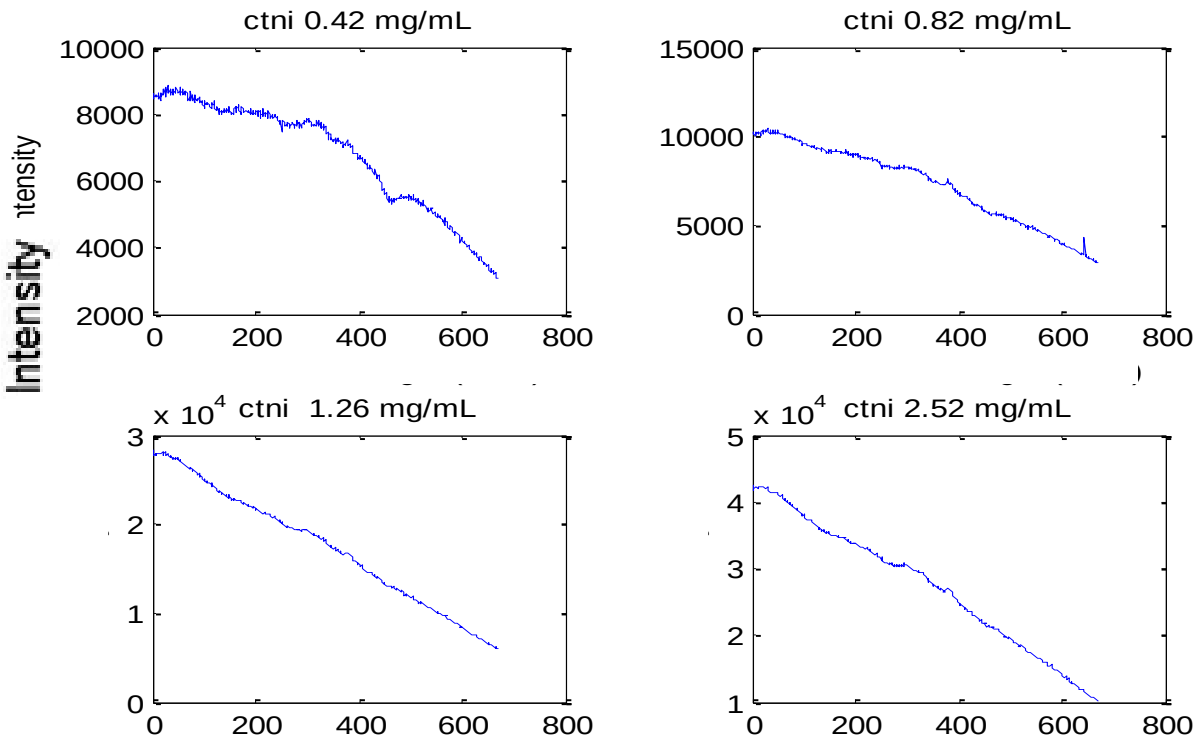

Figure 44: Water subtracted from new cTnI

From the above graphs it is evident that as the concentration of the cTnI increases the spectrum amplitude also increases, but it should also be noted that the amplitude increase is not linear with respect to the increase in concentration.

Figure 45 presents the effect of changes in concentration on the amplitude of spectra for the old cTnI samples and Figure 46 presents each concentration of old cTnI separately when water spectrum is subtracted from the signal. These samples are about two years old but have been stored in frozen powder form. Several factors such as occasional heating and cooling of the samples may have caused a portion of the proteins to be denatured. Moreover, from the acquired signals we can concluded that there are more impurities which may potentially cause florescence signal and to quench the Raman signal. The effect of the fluorescent signal is not visible in these samples.

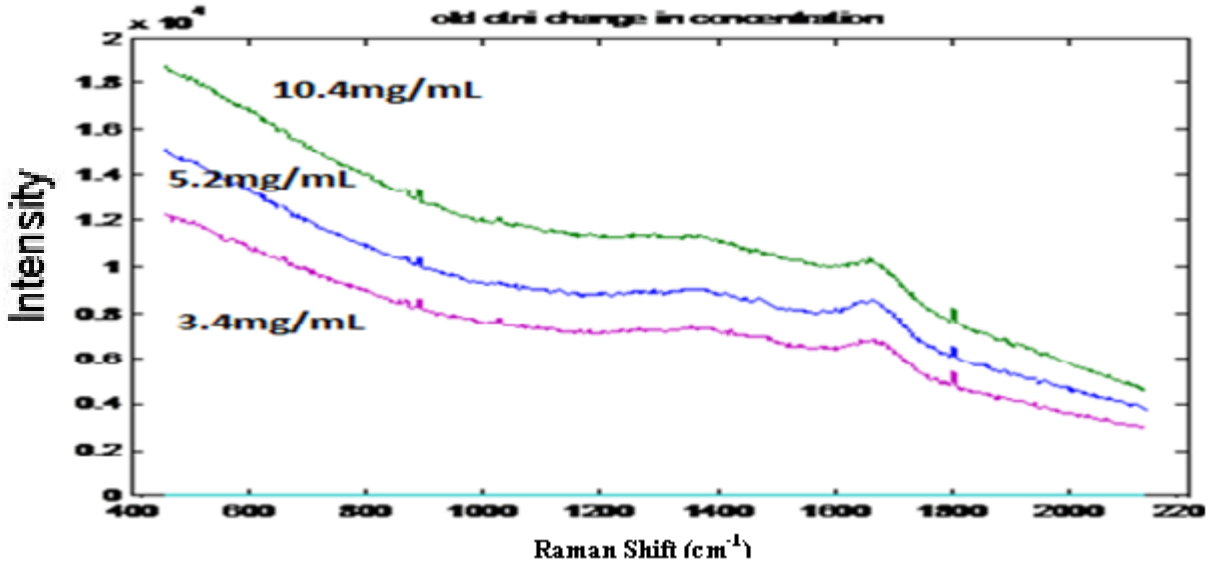

Figure 45: New cTnI Raman intensity for change in concentration

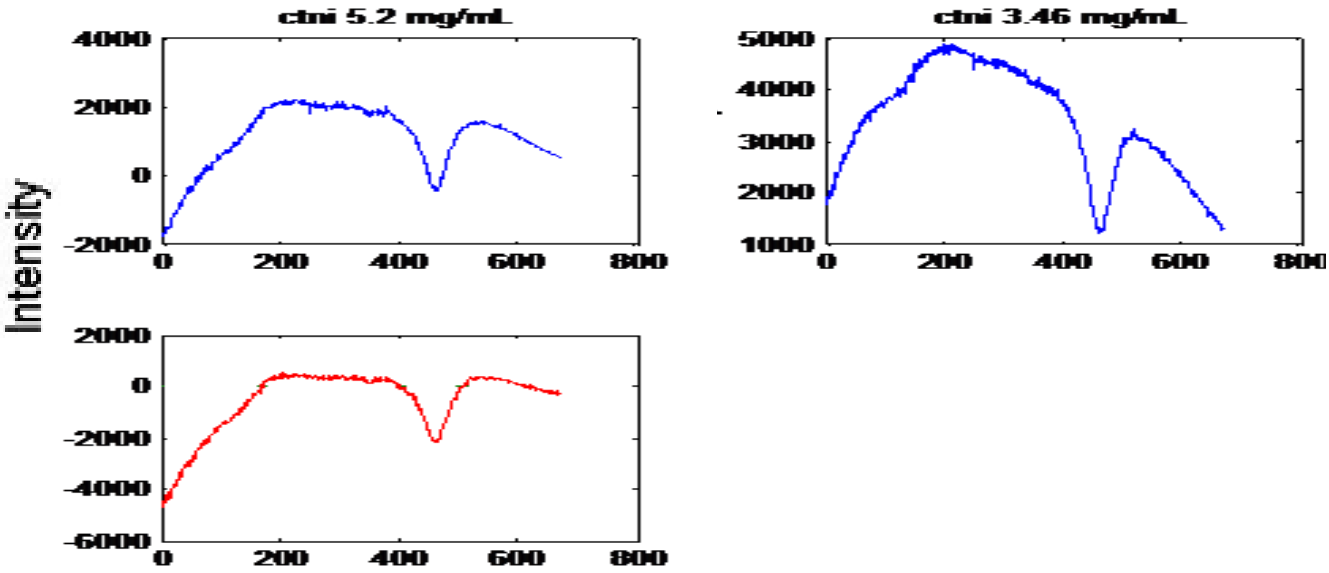

Figure 46: Old cTnI subtracted from water

From Figures 44 and 46 by subtracting water from the Raman signal we can evaluate whether or not there are characteristics to be detected from the subtracted signal that is associated with cTnI protein. Even though the signal characteristics are low in magnitude, after processing the signals and acquiring more precise instrument (more sensitive CCD), it is possible to characterize these peaks.

In the next set of results, signals from both new and old cTnI samples are analyzed. First Polyfit of the spectrum was subtracted from the raw signal using Matlab™ polyfit function as shown in Figure 47 and Figure 48. Both the polyfit with the raw signal and the signal with water subtracted were utilized, but the resulted graph form the latter was not as easy to analyze as the former. One reason for this again would be the presence of florescent contaminants in the signal. Moreover, after reviewing papers that have presented the same type of analysis and confirming with other graduate students working with other proteins on the same spectrometer, we have found the polyfit analysis of the raw data to be the conventional way to analyse the Raman data of a very low intensity signal characteristic level.

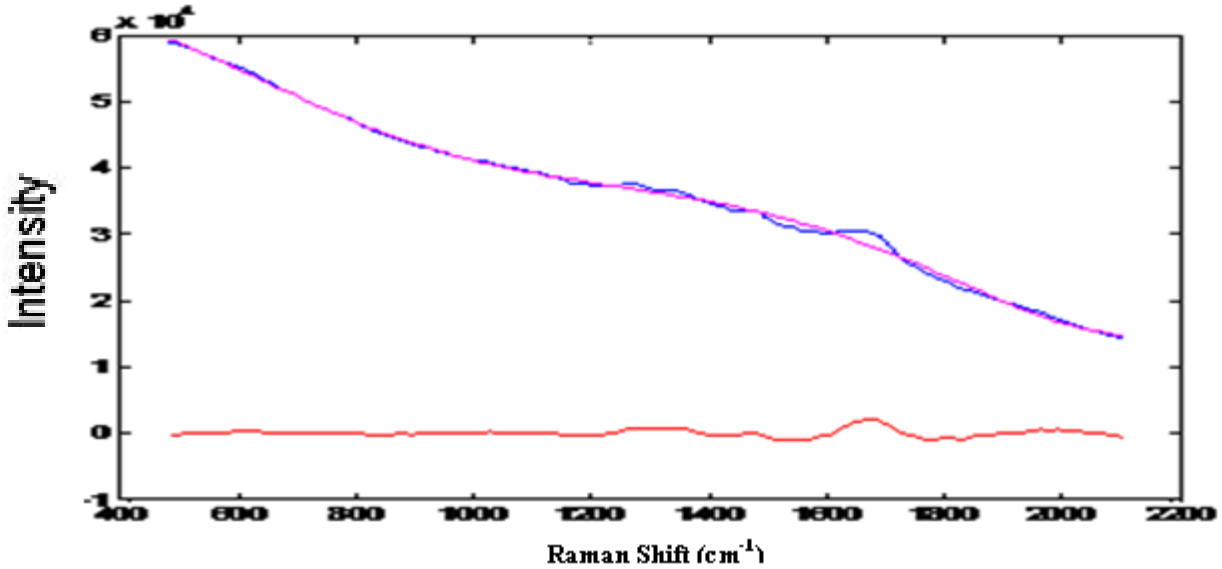

Figure 47: Polyfit subtraction steps for new cTnI.

In Figure 47(above), the pink graph (polyfit data) is subtracted from the blue graph (raw data) and the resulting graph is the red graph, which is also shown in Figure 48.

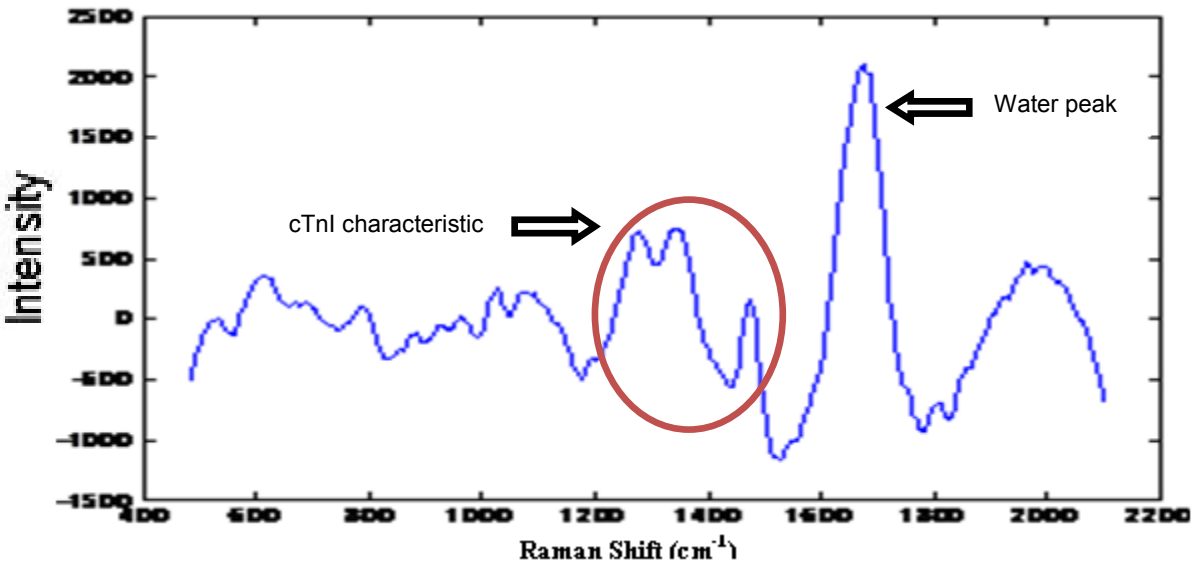

Figure 48: Polyfit subtraction result zoomed for new cTnI.

Next Savitzky–Golay (SG) smoothing tools were used to denoise the data. Using *sgolay()* function in Matlab the green curve/line in Figure 49 is produced. Then this graph is subtracted from the previous polyfit graph to remove the baseline, which is shown with a red curve/line.

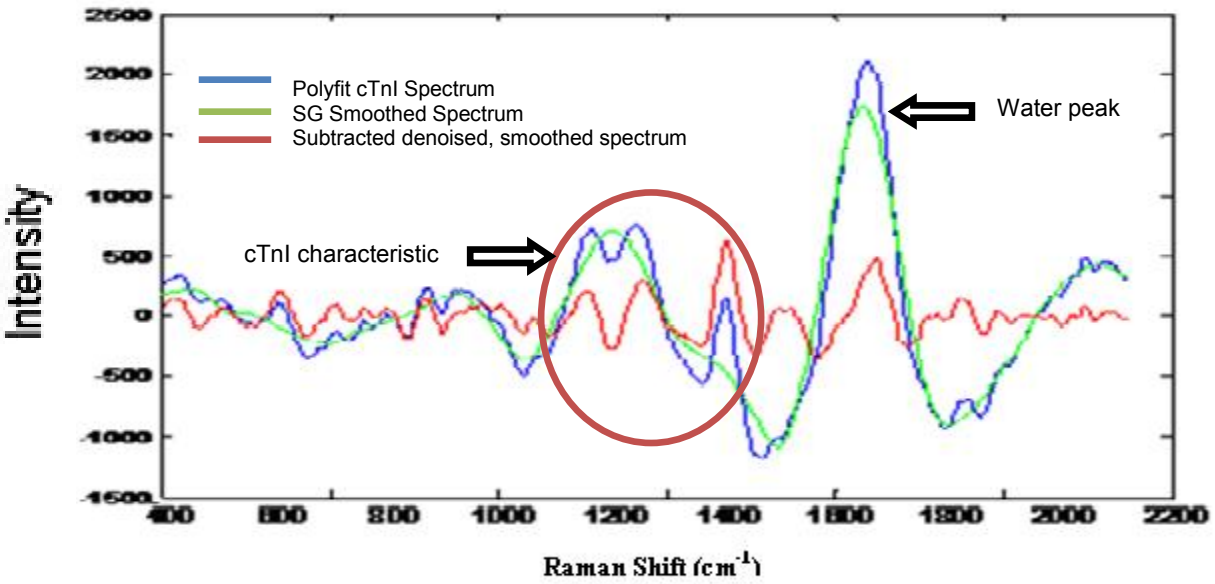

Figure 49: SG Smoothing process for the new cTnI

Figure 50 presents the processed data for increasing concentration of new cTnI samples. It can be noted from the graph that the signal intensity increases as the concentration of cTnI is

increased. However when the concentration of the protein is increased by 10 fold, the signal intensity does not increase by the same amount. Raman spectroscopy is both a quantitative and qualitative technique which is similar to a unique fingerprint of any molecule or substance. For quantitative measurements of Raman spectroscopy of a molecule chemometric methods can be used to further for higher concentrations of the sample to find the signature of the protein. As previously mentioned, fluorescence can often contaminate Raman spectra. The use of a Near-IR 785 nm laser helps in reducing the possibility of fluorescent contamination, but in the case of our samples, there is still a relatively large portion of fluorescent in the signal. Such contaminations can cause photo bleaching and saturation and result in the Raman signal to be quenched.

Therefore, even though we can conclude that cTnI Raman is quantitative, the relationship between the change in concentration of cTnI and its Raman signal is not linear and the intensity increase with the change in concentration is not very evident which again calls for more sensitive detection. The peak at 1700cm^{-1} is Raman peak for water and the peaks between 1200-1300 cm^{-1} are related to cTnI Raman signature.

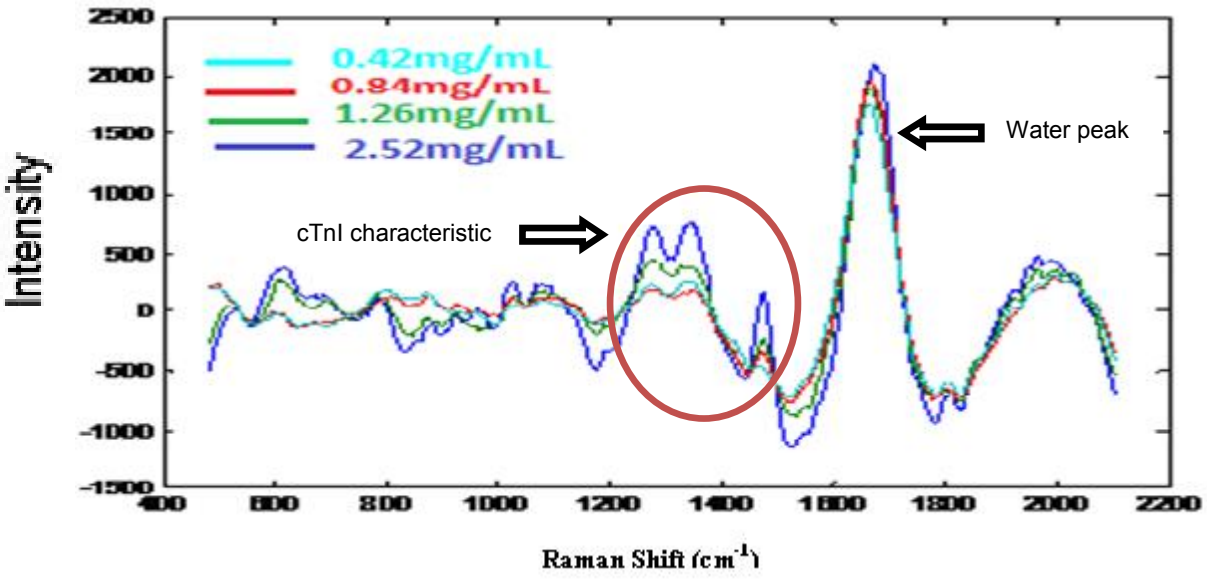

Figure 50: Increase in concentration for new cTnI, water not subtracted

Figure 51 presents the same SG smoothing step as above for the old cTnI and Figure 58 shows how the Raman spectrum of old cTnI changes as the concentration of the protein is increased. Again when the concentration of the protein is increased by 20 fold, the signal intensity does not increase by the same amount and we can conclude that the Raman signal is not linear. The same arguments for Figure 50 are also valid for the following figures.

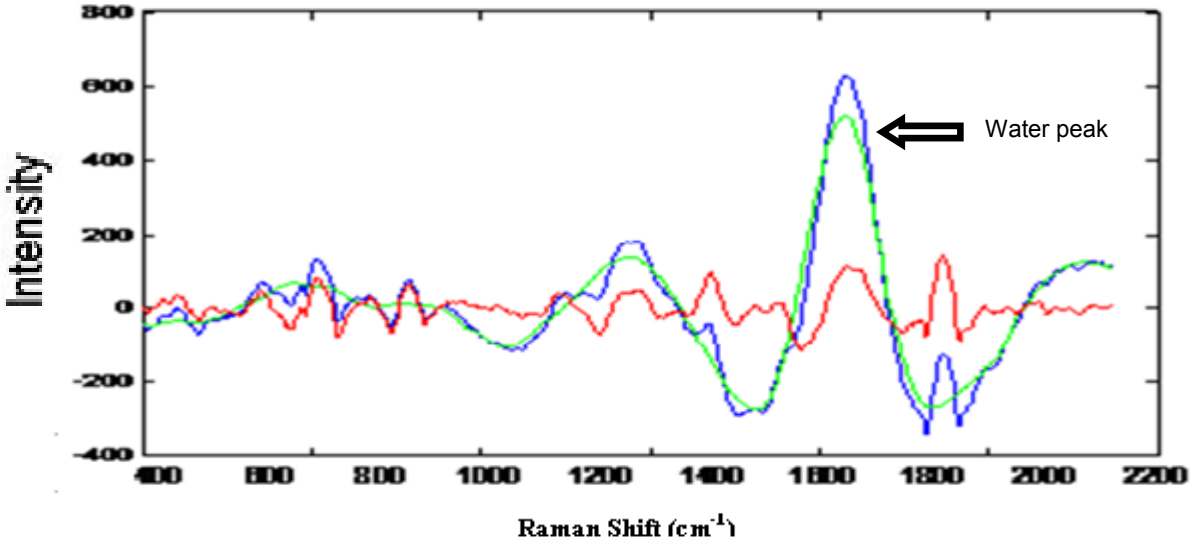

Figure 51: SG Smoothing process for the new cTnI

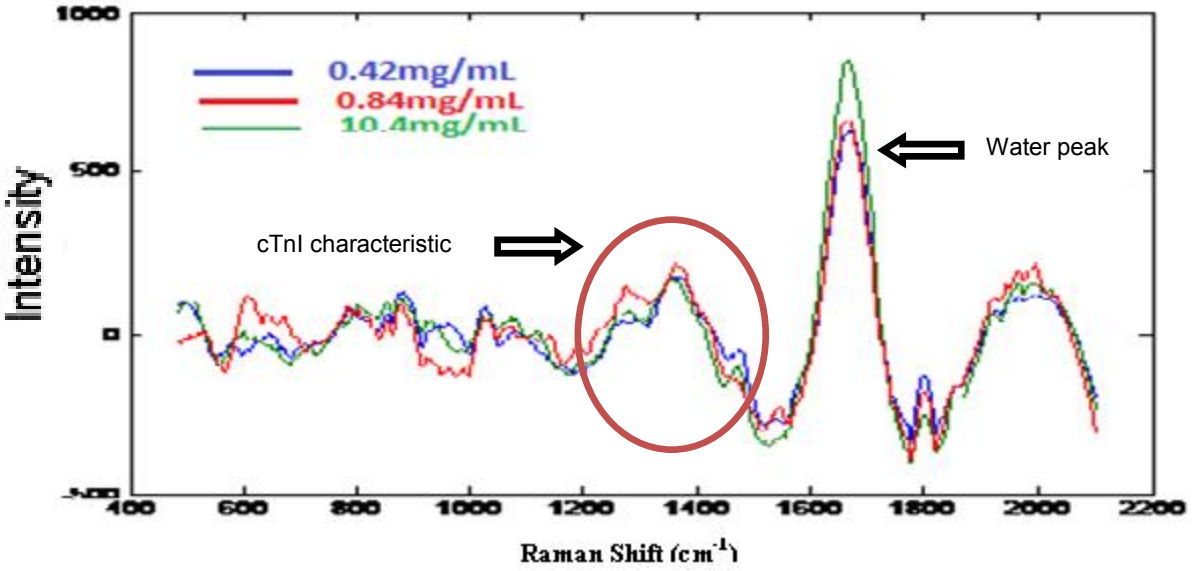

Figure 52: Increase in concentration for new cTnI

Figure 58 is an overlay of both old and new cTnI spectra for various concentrations. The red signal is from the new cTnI and the green signal is from the old cTnI samples. The peak with the highest intensity is water.

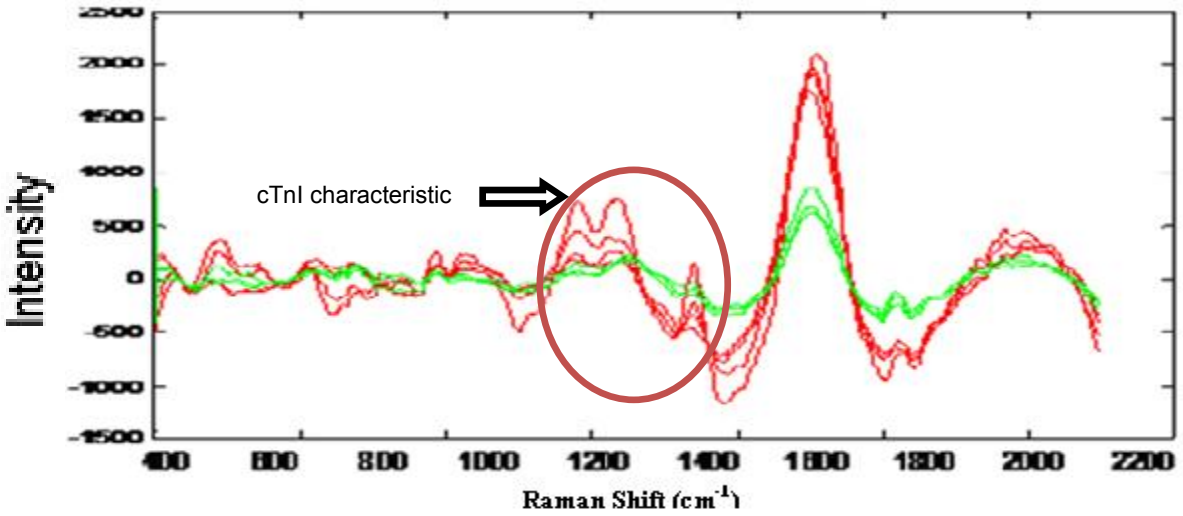

Figure 53: New and Old cTnI overlay

It can be noted from Figure 48 and Figure 50 that the Raman intensity changes as the concentration changes but for lower concentrations of cTnI the concentration change is not as much as concentration change in higher concentrations. The spectrometer that we use does not block the florescence signals therefore; at lower concentration of the protein, we receive more fluorescence signal than Raman signals.

From the above graph, it can be noted that even though the concentration of the old cTnI samples were higher than the newer samples, the intensity is lower. A possible explanation for this is that the amount of impurities was larger and there was more denaturation of the proteins in the old cTnI samples. Moreover, the indicated cTnI characteristic areas are believed to be unique to the protein.

3.4 Surface Enhanced Raman Spectroscopy

In this section Surface Enhanced Raman Spectroscopy (SERS) is investigated. SERS originates from the improved inelastic scattering of the molecules absorbed on nanostructured metals and alloys [22]. SERS is surface sensitive technique that results in the enhancement of Raman scattering by molecules adsorbed on rough metal surfaces. The enhancement factor can be as much as one petametre, which allows the technique to be sensitive enough to detect single molecules [22]. The main purpose of incorporating this method to the research is to characterize the Raman spectrum of cTnI, as this method will enhance the characteristic of the protein and will insure that the signature is only related to the component of interest. The initial cTnI solution was prepared in water but since the water has been evaporated or transferred to the edges of the sample, the water peaks are not evident in the spectrum and signal is solely from pure cTnI. We used a gold plate for this experiment. The novelty of this research is driven by the fact that there is no evidence of previous Raman analysis on cTnI in the literature. The raw spectra and its corresponding wavelet transform are shown in Figure 54 and Figure 55 respectively. The sample concentration used in all results in this section is 0.3 mg/ml.

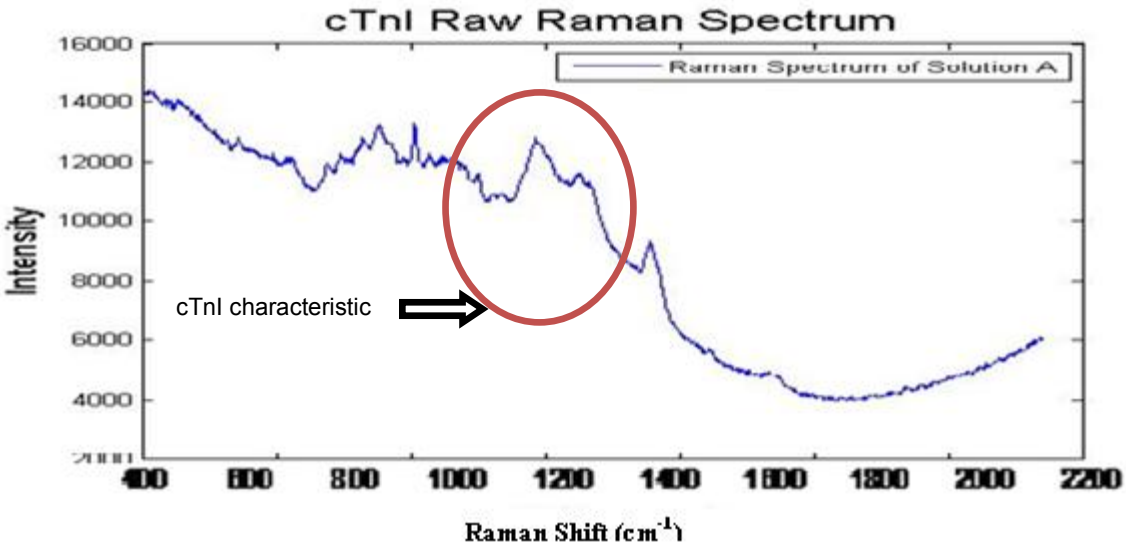

Figure 54: cTnI Raw Raman Spectrum

From Figure 59 we can observe that the same characteristic are again evident from the protein, which is further, makes our observation stronger. It should be noted that in SERS method water signal is not amplified and therefore not evident in the above graph.

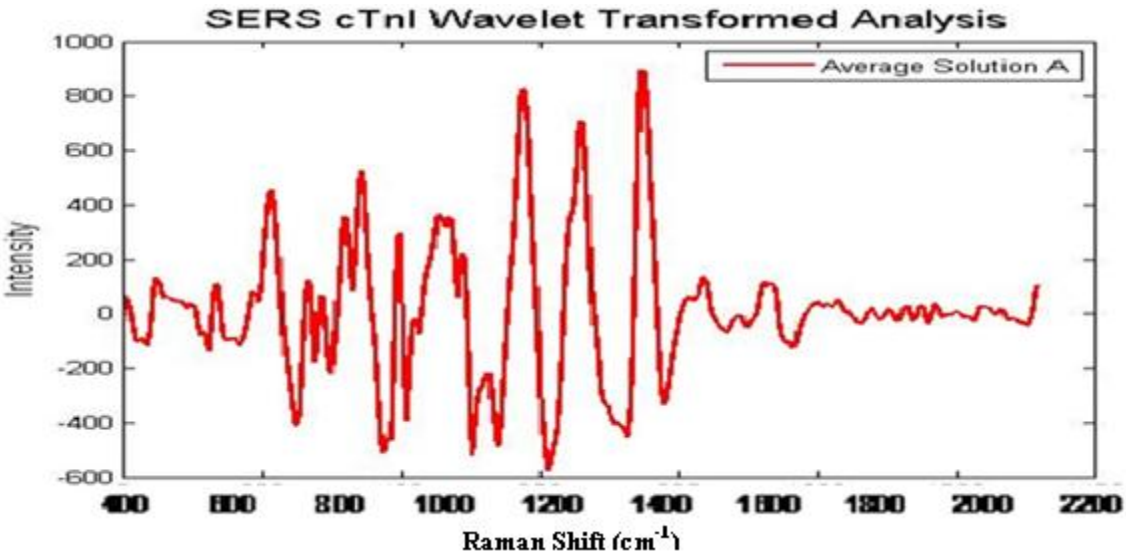

Figure 55: SERS cTnI Wavelet Transformed Analysis

As illustrated in the above graphs, the unique Raman spectrum of cTnI is extracted for future detection purposes. Figure 56 presents several iterations of SERS result of cTnI. One

reason for the error resulting from different intensity outcomes for the same sample can be due to the non uniform concentration of the protein on the gold slides.

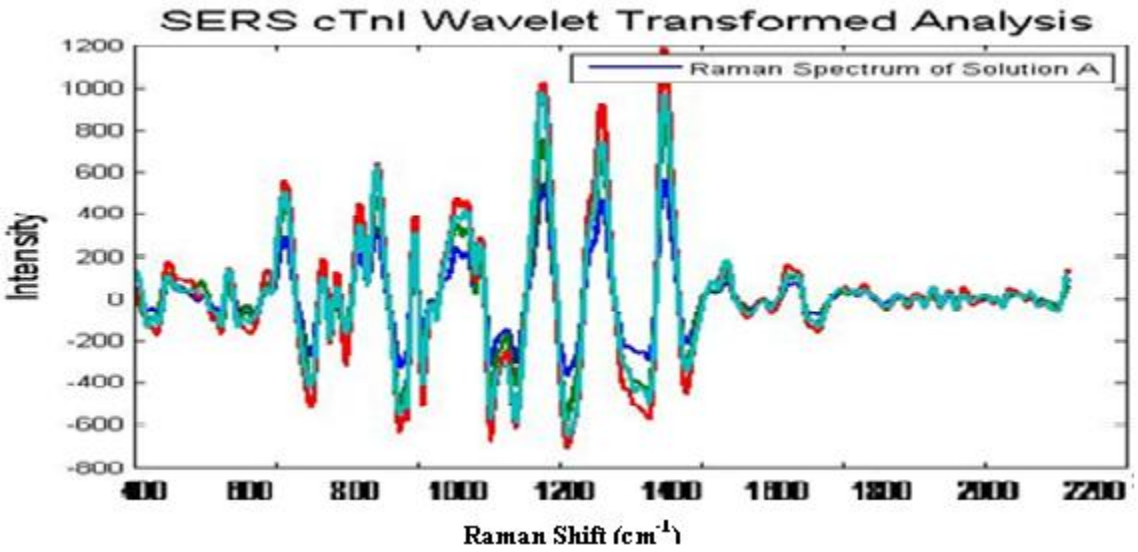

Figure 56: SERS cTnI Wavelet Transformed Analysis

Using SERS, the true Raman spectrum of cTnI could be extracted even with the lack of sensitive detectors as the signal is enhanced to a great degree. Although the implementation of SERS method in the actual *in vivo* system would not be possible, the processed spectra of cTnI signature using SERS will be used as a standard to compare future signals using high sensitive detectors.

It is evident that the signals acquired in water are to a large degree lower than the SERS spectra intensity. In addition, the intensity of the lower concentrations of the sample does not show linear relationships. It is possible that the lower concentrations of the samples result in the weakening of Raman signals and the disappearing of some weak Raman spectral peaks. That may be because when the sample is dissolved into the water, the crystal structure is broken, and for some samples, this event may cause formation of ionic solution.

4: RAMAN SPECTRSOCPY OF THE RETINA

4.1 Conceptual Design of Raman Detection of cTnI System

The focus of this research so far has been on finding the Raman spectrum of cTnI. The last part of the proceeding research is based on designing a conceptual proof of concept design for a device to be used as Raman spectroscope for measuring cTnI from the eye. Figure 57 shows various parts of eye anatomy, which can be used as access point to the blood. Because through the back of the eye we can get direct access to a pool of fresh blood from the heart, this organ can be used as a suitable measuring site for the purpose of this project. Moreover, the transparent characteristic of the eye adds to its advantage as a collection site.

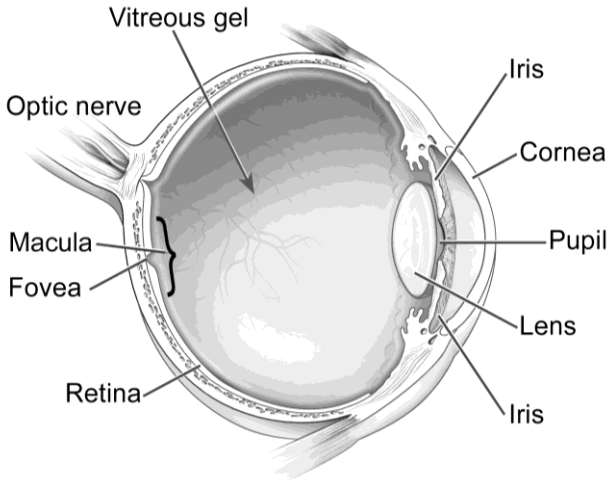

Figure 57: Anatomy of the eye (With permission from [23])

From Figure 58 it can be seen that the optic nerve has the most concentration of blood vessels and has the highest potential for accessing blood. Furthermore, the laser will be less damaging to the vision at this site as there are no photosensitive cells (it is the “blind spot”).

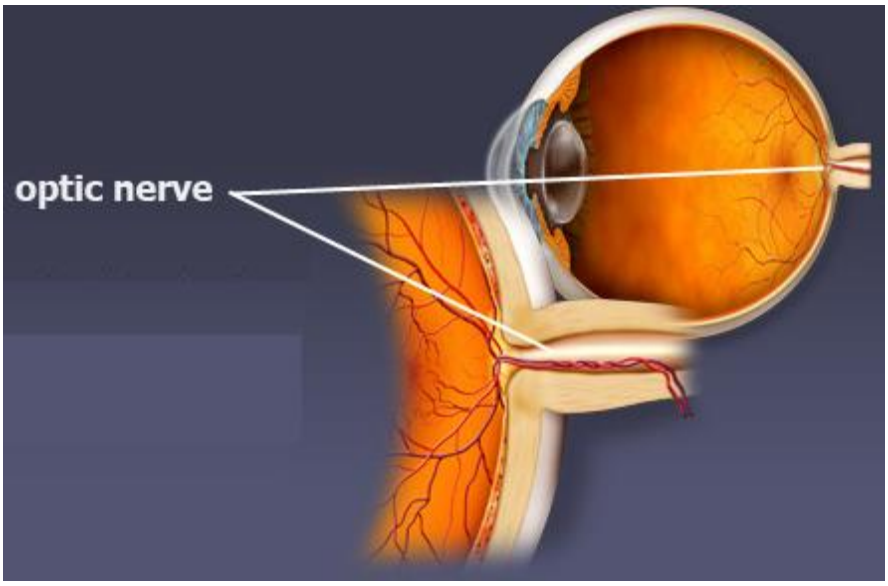

Figure 58: Optic Nerve, Sampling point of interest (Modified from [24])

One possible configuration for the purpose of our proof of concept is combination of Raman and confocal Scanning Laser Ophthalmoscopy (cSLO). The technique behind cSLO is to raster scan laser beam, focused to a spot of approximately 0.1mm, over the surface of the retina. [27] The main advantage of the cSLO system for the purpose of this research is the ability of the confocal configuration to block signals that are not coming from the blood vessels in the retina. In addition, this configuration will provide testability of the system and information about whether it is focused on the right place and allow for evaluation of the system performance. Also this configuration will result in a cleaner signal.

Figure 59 is a schematic of a simplified and modified cSLO system used to image human eye. A modified version of the schematic presented in Figure 65 can be used for the prototype. A laser beam from a laser source is focused onto the retina by the refractive components of the eye (the cornea and lens). The corresponding back reflected light passes through the system and is focused through a pinhole and detected by a detector such as Avalanche Photo Diode (APD). The confocal pinhole provides a level of depth selection. It rejects the light originating from

outside the depth of focus. In the following SLO layout the M stands for mirror and BS stands for beam splitter.

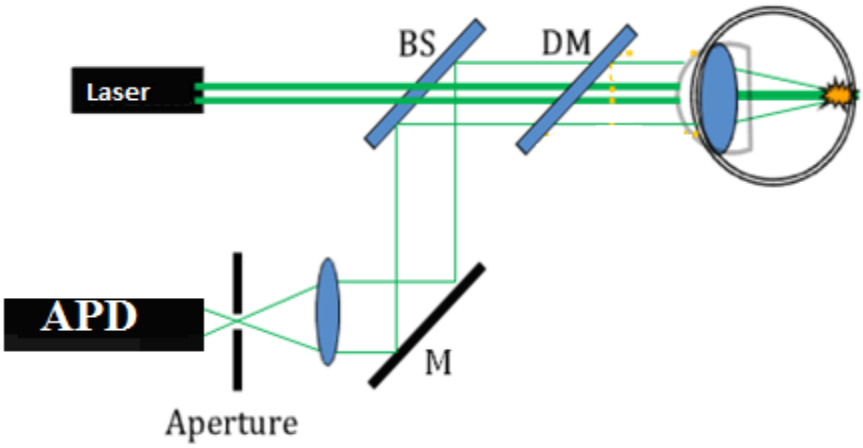

Figure 59: Schematic of simplified SLO system used to image human eye (With permission from [23])

Figure 60 presents a possible Raman spectroscopy configuration in the eye. In this configuration, DG stands for Diffraction Grating, LPDF for Long Pass Dichroic Filter, and BP for Bandpass Filter. A modified version of the schematic presented in Figure 65 can be used in the final prototype and for testing the system.

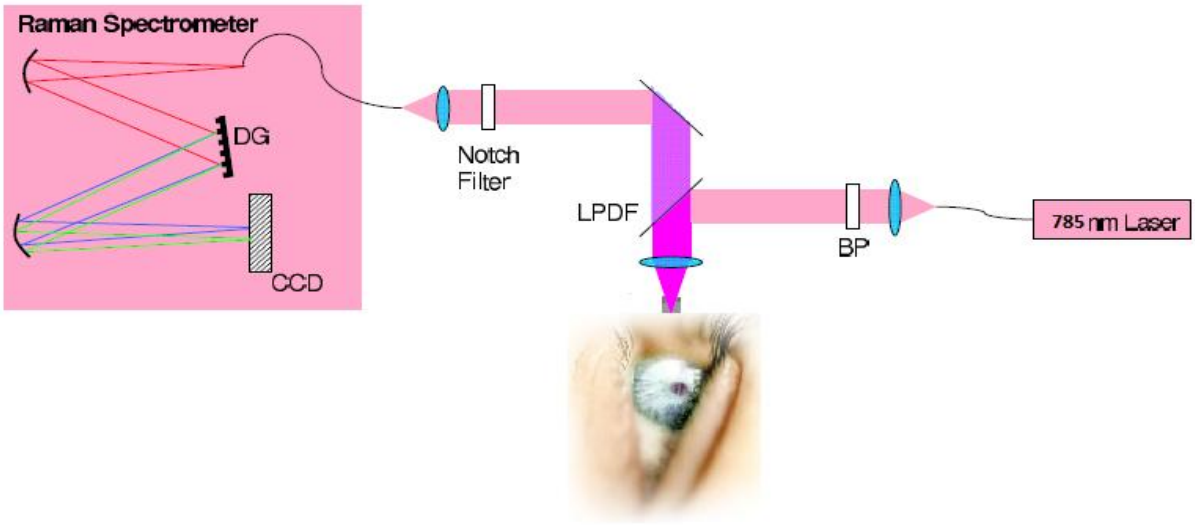

Figure 60: Possible Raman Spectroscopy configuration for conceptual system (Modified from [25])

Another add-on option for our SLO/Raman configuration is to have a beam scanner sub system to find a blood vessel in the mouse eye before starting the measurement. This add on configuration is presented in Appendix III. It should be noted that the difference between Figure 36 diagram from a US patent and our configuration is that the former is a full field whereas the latter laser is focused to a point.

Figure 61 presents a combination of subsystems which can be used as our conceptual design and only uses Raman spectrsocopy. A version of the system that incorporates both SLO and Raman configurations is presented in Appendix IV which is the modified version of Figures 60 and 59 combined for human eye for the purposes of testing and prototyping. The sample arm is used to find the point of interest to focus on, which in this case will be the blood vessels near the optic nerve. The purpose for the confocal SLO is to locate acquisition point when acquiring SLO image. Hypothetically, these results can be compared to the results from the blood vessels on the adjacent regions.

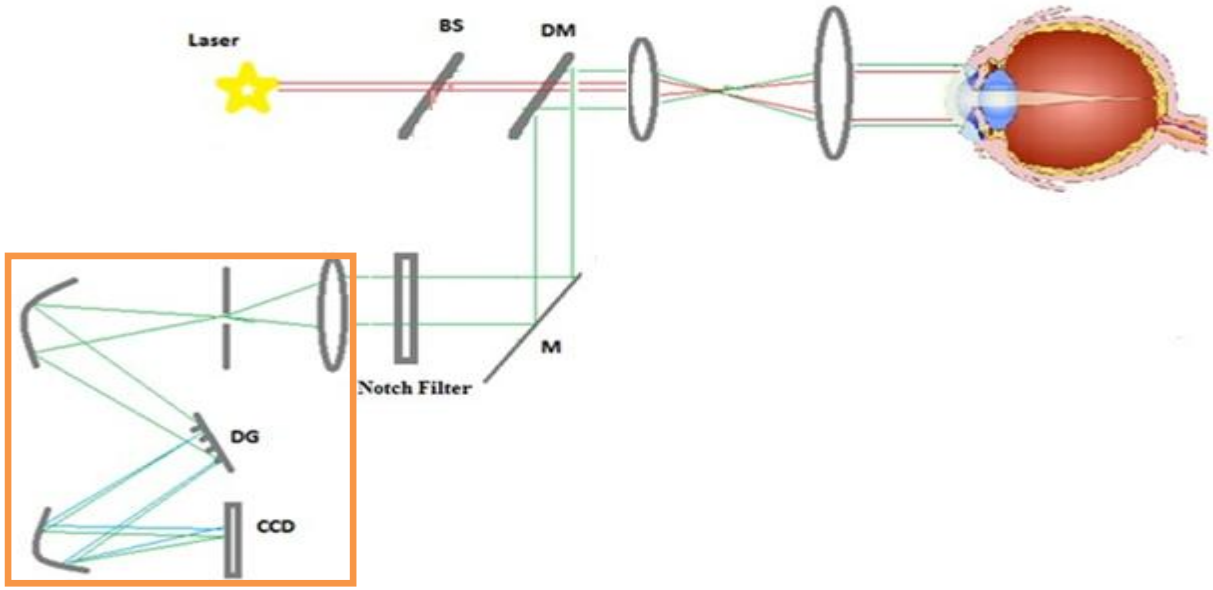

Figure 61: Overall Conceptual Optical Configuration

Figure 62 presents an overall conceptual design of the system. The excitation beam will be transmitted (in short pulse form) from a small laser diode through the pupil and to back of the retina and more specifically on the optic nerve. Consequently, the emission light is reflected back through the pupil and to a small prism, which in turn will reflect the light to a miniaturized CCD camera for measurement. The processing of the spectra will be performed on a separate unit similar to the ECG processing unit presented in Chapter 1 of this research.

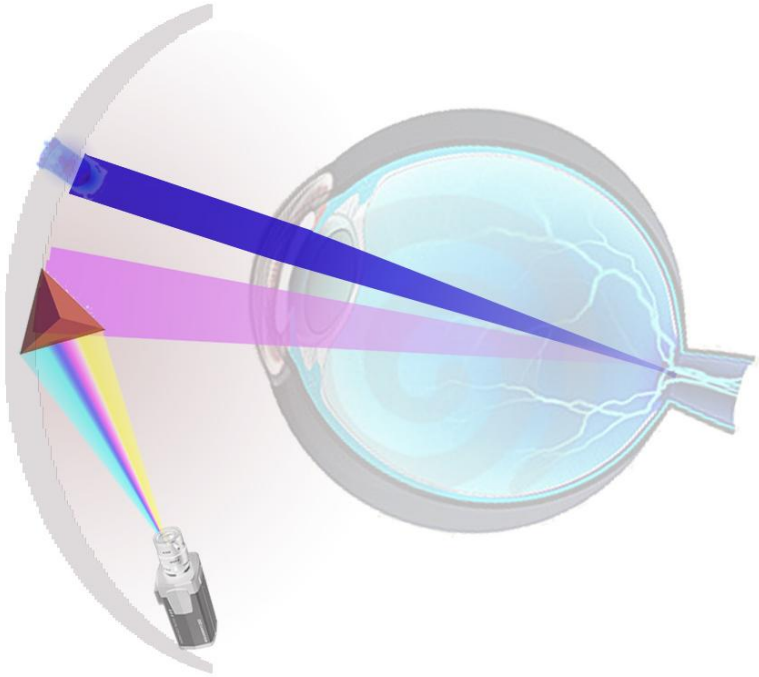

Figure 62: Conceptual Design

4.2 Maximum Permissible Exposure in the Eye

It is very important to assess our constraints and limitations when designing the system. The most important limitation is dictated by the maximum permissible laser exposure in eye. Table 6 summarizes the steps on finding the maximum permissible exposure (MPE) in the eye for the purpose of our project. The table shows the calculations of MPE for wavelength between 700-1050 nm. The Raman spectroscope we have been using for our experiments employs 786nm laser. The advantage of working with longer wavelengths is that generally for longer wavelength, higher the MPE can be obtained. This is useful for imaging the back of the eye as long as we stay below the strong water absorption in the vitreous.

On the other hand, in order to minimize the exposure of the eye to continuous laser power and consequently damage to the eye, we need to use short pulses. The repetitive pulse limit MPE/Pulse suitable for our purposes is 260 W/cm^2. For a spot size of 1 mm on the cornea, the average and single pulse power on the eye that is acceptable is:

Average MPE for duration of the exposure:

MPE_{Group} for 1 mm^2= 0.0148 W/mm^2 *0.01 mm^2=147μW

Average Single Pulse MPE:

MPESP (W/cm^2) = 89μW

Repetitive pulse limit MPE per pulse:

MPE /pulse (W/cm^2) = 158μW

The average powers are surprisingly low, but it should be noted that we are using a 1mm spot size at the cornea, which will be focused to 20 μm diameter at the retina. The average MPE found above for single pulse duration of 5 second and complete exposure of 1 minute is very low for our current Raman spectrometer configuration we have used. So far, we have been using the continuous wave (CW) laser to get the Raman spectra. From the experiments conducted in the previous sections, we can see that in order to obtain MPE for our design we may not be able to get enough signal to noise ratio from our spectra. One option to increase sensitivity of our device and be able to maintain MPE is using EMCCDs instead of regular CCDs.

Table 6: Calculated MPE for 786nm

	Wavelength (nm)		**This table is valid for wavelength ranges from 700 - 1050nm**				**# of Pulses (Complete Duration x Pulse Frequency)**
Repetitive Pulse MPE	**786**		**Single Pulse Limit**	**Average Power Limit**		**Repetitive Pulse Limit**	0.1
PRF (Hz)	Single Pulse Duration (s)	Duration of Complete Exposure (s)	MPE_{SP} (W/cm^2)	MPE_{Group} (W/cm^2)	MPE_{Group} /Pulse (W/cm^2)	MPE/Pulse (W/cm^2)	**C_P (Correction Factor)**
0.0016	5	**60**	0.0089	0.00148	0.0148	0.0158	1.778
							C_A (Correction Factor)
Note: The lowest MPE/Pulse will be the limit of the power possible for the system.							1.479

5: CONCLUSION

This research started with evaluation of ECG signal for the purpose of predicting heart abnormalities and monitoring patients to decrease mortality rate caused by missed MI detection. Even though ECG is the traditional method for monitoring MI and has been used for a long time, this area is still underdeveloped and can be explored further, but our initial analysis indicated that ECG is not a sufficient predictor of MI due to large probability of false positive and false negatives as these signals are most sensitive to neurological nature of heart attack (arrhythmia). Also in most cases by the time the ECG signal starts to indicate abnormal heart activity, the damages to the heart are irreversible and heart attack has already occurred. Moreover the probability of false positive and false negative in ECG abnormality measurement is high relative to immunoassay measurements.

For these reasons we moved on to a biophotinc measurement. The first approach was florescence spectroscopy. Because of an existence of Tryptophan amino acid in cTnI sequence, this protein has florescence characteristics. After a complete analysis on florescence spectroscopy of the protein, we have concluded that this method does not provide any unique information on the protein structure with the available technology. Although the above techniques were not successful, they provide a great deal of information which can be used for the future designs that can be used in parallel with the approaches and act as a complementary method. Moreover, other cardiac biomarkers besides cTnI were studied in this research and their incorporation in the final system will complement the specificity of the result attained by monitoring cTnI.

To summarize the major results of this work, we have assessed the possibility of measuring the Raman spectra of cTnI protein in the blood. First cTnI was diluted in several buffers and its Raman signature was found. One of the main constrains of this research is the low biological concentration of this protein in the blood and the very low signal to noise ratio of the attained signals. Therefore the concentration used for these experiments are 10 times higher than biological levels in the blood. Water was used as the medium for the Raman spectroscopy experiment as there was barely any Raman signal from the cTnI in the blood because of its low concentration and signal comparing to other blood component. Moreover there was no evidence of previous Raman signature of cTnI in the literature, which caused a lack of frame of reference to compare the obtained peaks in order to enhance the overall spectrum. It should be noted that the Raman signal is approximately 10^{-6} to 10^{-7} lower that the excitation signal in magnitude therefore the sensitivity of the detection system is the main drawback of this research. In the future, using EMCCD instead of regular CCD can possibly increase the signal-to-noise ratio and lower concentrations can potentially be detected. Next, the measurements were repeated for several concentrations of the protein and all the signals were analyzed. The resulting graphs showed an unexpected non- linear correlation between Raman signal and cTnI concentration in the buffer. The main achievement and the novelty of this research is driven by the fact that there is no evidence of previous Raman analysis on cTnI in the literature and we have been able to obtain and extract the first Raman spectrum of cTnI.

The second part of this research was focused on designing a conceptual Raman/SLO configuration as part of instrumentation study of the system. The future

work on this project can be performed on improving the signal detection and miniaturization. Most importantly before any further investigation, a more complete feasibility study should be performed on how to enhance the signal using spectrometers with stronger CCDs. Next the development and optimization phase of the design for the cTnI monitoring device can be started.

Moreover the preliminary part of this research study on a telemedicine ECG measurement device can potentially be incorporated into the final design of the narrowly specialized Raman spectrometer for a complete non invasive diagnosis of more comprehensive types of Coronary heart diseases.

6: APPENDICES

6.1 Appendix I

6.1.1 Sample Preparations

The following steps were followed for sample preparation of cTnI in various buffer solutions for generating noise.

Buffer solution:

0.1M, KH2PO4 – 0.1M, NaOH, pH (6.0;7.0; 8.0).

200mL of Buffer

0.1 M KH2PO4 (136.09 g/mol)→2.72gr

0.1 M NaOH (40 g/mol)→ 0.8gr

PH 7.2

1 L of Buffer

0.1 M KH2PO4 (136.09 g/mol)→13.6gr

0.1 M NaOH (40 g/mol)→ 4gr

Mixing

Add 2Mercato Ethanol (14.2 M) → to reduce disulfide linkages

Working Concentration: 7mM

CiVi=CfVf→ Vi=0.49mL

Dialysation at the cold room

cTnI 25KA

cTnT 35KA

Cut Off 14KA

Optima TLX Ultracentrifuge

30000RPM for 30 Min at 40 deg

TLA 45 Rotterhead

Max 45K RPM

A280:

cTnI: 0.111 :c=0.49g/L

cTnT: 0.233: c=0.25 g/L

Stock Solution 0.01g/L

BSA (SIGMA: A 7888)

Mol wt ~66KDa

PH 5-5.6 (1% in H2O)

Temp 2-8 deg

cTnI: 0.1x10e-9g/ml

Albumin Physiological Value: 0.45g/mL

After making solutions, the concentrations where measured using nanoDrop™ spectrometer. Figure 68 presents an example of the concentrations measured using the device.

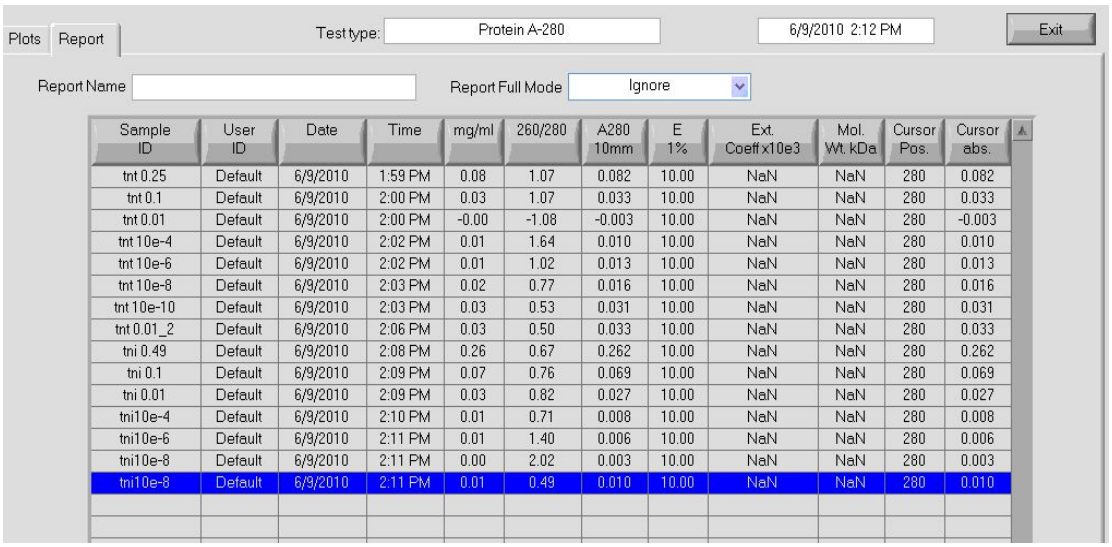

Sample ID	User ID	Date	Time	mg/ml	260/280	A280 10mm	E 1%	Ext. Coeff x10e3	Mol. Wt. kDa	Cursor Pos.	Cursor abs.
tnt 0.25	Default	6/9/2010	1:59 PM	0.08	1.07	0.082	10.00	NaN	NaN	280	0.082
tnt 0.1	Default	6/9/2010	2:00 PM	0.03	1.07	0.033	10.00	NaN	NaN	280	0.033
tnt 0.01	Default	6/9/2010	2:00 PM	-0.00	-1.08	-0.003	10.00	NaN	NaN	280	-0.003
tnt 10e-4	Default	6/9/2010	2:02 PM	0.01	1.64	0.010	10.00	NaN	NaN	280	0.010
tnt 10e-6	Default	6/9/2010	2:02 PM	0.01	1.02	0.013	10.00	NaN	NaN	280	0.013
tnt 10e-8	Default	6/9/2010	2:03 PM	0.02	0.77	0.016	10.00	NaN	NaN	280	0.016
tnt 10e-10	Default	6/9/2010	2:03 PM	0.03	0.53	0.031	10.00	NaN	NaN	280	0.031
tnt 0.01_2	Default	6/9/2010	2:06 PM	0.03	0.50	0.033	10.00	NaN	NaN	280	0.033
tni 0.49	Default	6/9/2010	2:08 PM	0.26	0.67	0.262	10.00	NaN	NaN	280	0.262
tni 0.1	Default	6/9/2010	2:09 PM	0.07	0.76	0.069	10.00	NaN	NaN	280	0.069
tni 0.01	Default	6/9/2010	2:09 PM	0.03	0.82	0.027	10.00	NaN	NaN	280	0.027
tni10e-4	Default	6/9/2010	2:10 PM	0.01	0.71	0.008	10.00	NaN	NaN	280	0.008
tni10e-6	Default	6/9/2010	2:11 PM	0.01	1.40	0.006	10.00	NaN	NaN	280	0.006
tni10e-8	Default	6/9/2010	2:11 PM	0.00	2.02	0.003	10.00	NaN	NaN	280	0.003
tni10e-8	Default	6/9/2010	2:11 PM	0.01	0.49	0.010	10.00	NaN	NaN	280	0.010

Figure 63: Concentrations measurement using nanoDrop™

6.2 Appendix II

6.2.1 Initial Raman Spectroscopy Results

In order to investigate the possibility of cTnI detection using Raman spectroscopy two experiments were designed and conducted. For the first experiment a commercialized SpectraCode RP-1 Portable Raman Spectrometer was used. Figure 64 presents the spectrum of water which was used as negative control for this experiment.

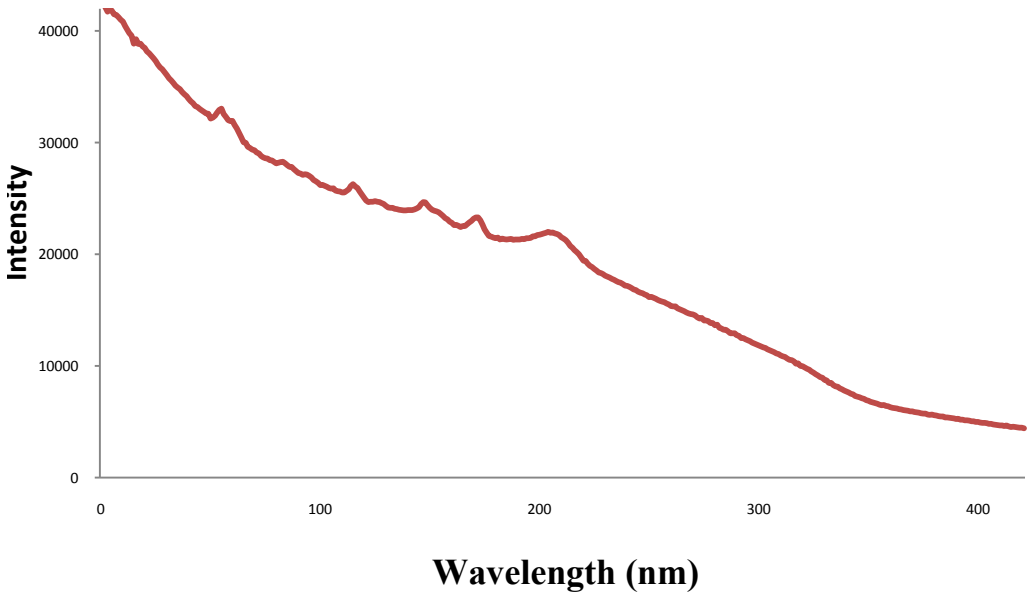

Figure 64: Raman Spectroscopy of Water

Five µg of cTnI was diluted in 3mL of water and the concentration of the solution was decreased iteratively from 0.78 mg/mL to 0.60 mg/mL and spectra were acquired .

For the second experiment cTnI sample was prepared and was diluted in Tn Complex Buffer. The initial concentration of cTnI in Tn Complex buffer was 2.47 mM. Tn Complex Buffer was selected due to its similarity to serum for the purpose of cTnI dilution to prepare different concentrations. For this experiment a LABRAM

Spectrometer was used. The instrument consists of three parts: an internal HeNe (633nm) laser, a microscope, and a spectrometer.

Figure 65 presents change in concentration of cTnI in Tn complex. As expected it can be concluded from Figure 65 that the Raman signal intensity of cTnI decreases in the water or Tn Complex as the sample is more diluted which makes Raman Spectroscopy a promising method for detection of cTnI in the serum.

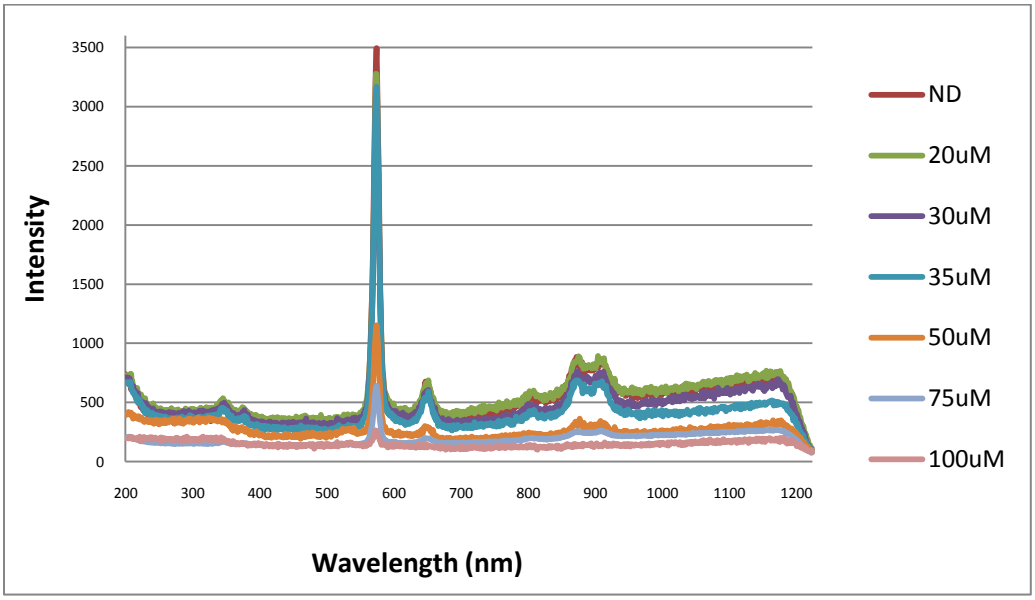

Figure 65: Raman Spectroscopy in Tn Complex

Appendix III

6.2.2 Beam Scanner Sub System

The labels f1, f2, f3 are the focal lengths of each of the lenses. A modified version of the schematic presented in Figure 66 will be used in our final design.

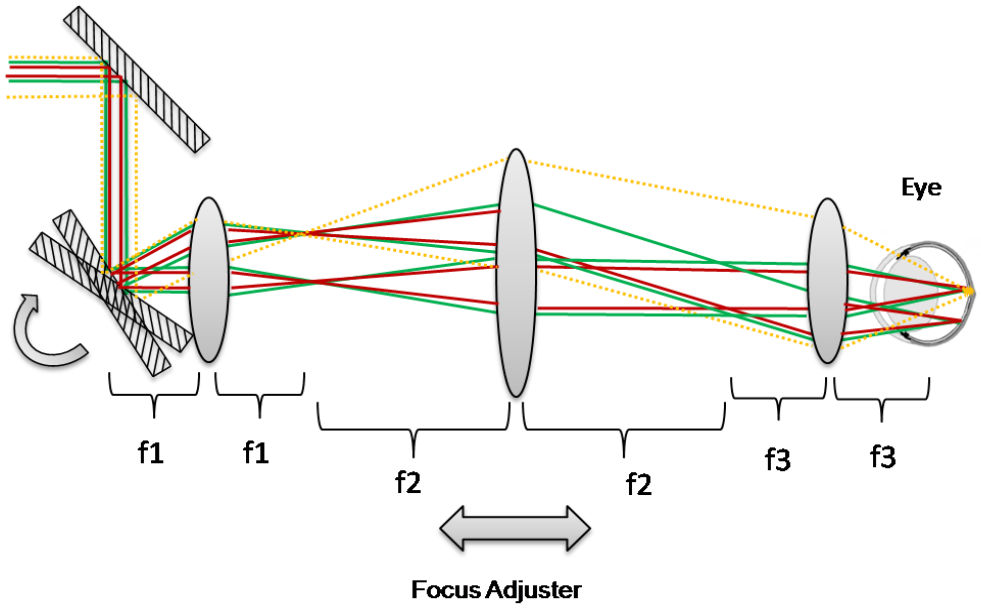

Figure 66: SLO Sample Arm configuration in mouse eye (With permission from [23])

6.3 Appendix IV

6.3.1 SLO/Raman Overall Conceptual Design

The following configuration presents an alternative presentation of the conceptual design with incorporates a SLO channel for more accurate imaging.

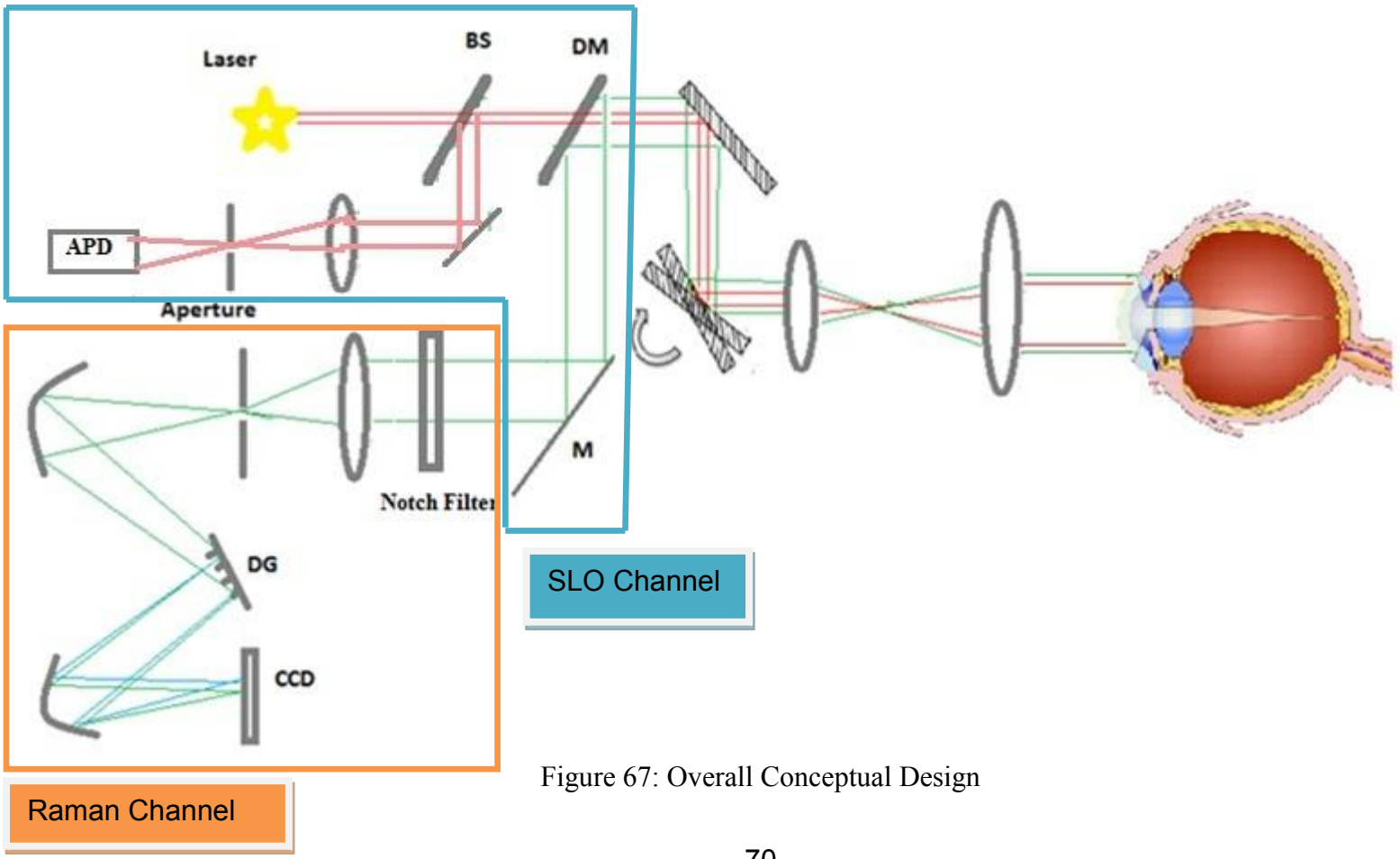

Figure 67: Overall Conceptual Design

7: REFERENCE LIST

[1] World Health Organization, "Deaths by cause, sex and mortality stratum in WHO regions," The world health report, 2004.

[2] Abbott Laboratories. "Diagnostic Value and Prognostic Potential of Cardiac Troponin," Illinois: Millennium Medical Communications, 2001.

[3] Hideo Hirose, K. K, "Diagnostic accuracy of cardiac markers for myocardial damage after radiofrequency catheter ablation. Journal of Interventional Cardiac Electrophysiology , 169-174. 2006.

[4] Katherine Soreng, P, "Troponin I and Troponin T in Myocardial Infarction Diagnosis and Risk Assessment".Tarrytown: Bayer HealthCare LLC, Diagnostics Division, 2006.

[5] A. Juliet, and Wolfe Barry, "Cardiac troponins: their use and relevance in anaesthesia and critical care medicine." The Board of Management and Trustees of the British Journal of Anaesthesia , 62-66. 2008.

[6] D. C., Collinson, "Multiple molecular forms of circulating cardiac troponin:analytical and clinical significance." Association for Clinical Biochemistry. , 349–355. 2008.

[7] "Solution Structure of Calcium-Saturated Cardiac Troponin C bound to cardiac Troponin I." J.Biol.Chem. 277: 38565-38570. 2002.

[8] V.R. Eisenman, "Are all troponin assays equivalent in the emergency department?" Singapore Medical Journal , 325-327. 2005.

[9] F. S., Apple. "Cardiac Troponin Testing for Detection of Myocardial Infarction." Minneapolis: Humana Press. 2008.

[10] E. A., Perry, " Enzyme-Linked Immunosorbent Assay (ELISA)." Sinauer Associates and Sumanas, Inc. 2002.

[11] Oxis International, Inc, "Troponin I (Human Cardiac-Specific) Enzyme Immunoassay Test Kit" Foster City,: Oxis International, Inc. 2002.

[12] Labmaster Ltd."Labmaster Troponin I ELISA:quantitative ELISA test." Turko: Labmaster Ltd. 2008.

[13] Lakowicz, J. R. "Principles of Fluorescence Spectroscopy." New York: Springer. 1999.

[14] Photon-Control.com. "Photon Control." Retrieved April 15 , 2009, from Spectroscopy Manufacturer, CCD Technology: http://www.photon-control.com/spectroscopy.html. 2009.

[15] Microscopy Resource Center. "Olympus Microscopy Resource Center." Retrieved April 15, 2009, from http://www.olympusmicro.com/primer/anatomy/sources.html. 2009.

[16] Clark, J. "Absorption Spectra-The Beer Lambert Law." Retrieved April 26, 2009, from The Beer Lambert Law: http://www.chemguide.co.uk/analysis/uvvisible/beerlambert.html. 2007

[17] D. M., Char, E. Israel, and J. Ladenson, "Early laboratory indicators of myocardial infarction," Emergency Medicine Clinics of North America, 1998.

[18] D. I., Ellis, and R. Goodacre, "Metabolic fingerprinting in disease diagnosis: biomedical applications of infrared and Raman spectroscopy," Analyst, 2006.

[19] Julia Evans et al. "Optical coherence tomography and Raman spectroscopy of the ex-vivo retina." Multimodal Biomedical Imaging IV, Proc SPIE. San Jose, CA, Vol. 7171, 13768-13784. 2009.

[20] Annika M. K. Enejder et al., "Blood analysis by Raman spectroscopy." Optics Letters , Vol. 27, Issue 22, 2004-2006.

[21] Anthony J. Durkin, M. N. Patent No. US 6,721,583 B1. United States. 2004.

[22] I.M. Vlasova, A.M. Saletsk, "Raman spectroscopy in investigations of mechanism of binding of human serum albumin to molecular probe fluorescein." Moscow: Lomonoaoy Moscow State University. Vol 5, Issue 5. 2008.

[23] Nima, Hossien-Javaheri, "Non-invasive retinal imaging in mice with fluorescent scanning laser ophthalmoscopy and fourier domain optical coherence tomography." Canada: Simon Fraser University. 2010.

[24] L.H. Qian et al. "Surface enhanced Raman scattering of nanoporous gold: Smaller pore sizes stronger enhancements. Appl. Phys. Lett. 90, 153120. 2007

[25] Nie, S.; Emory, S. R., Probing Single Molecules and Single Nanoparticles by Surface-Enhanced Raman Scattering. Science 1997, 275, (5303), 1102-1106

[26] National Eye Institude. "Eye Anatomy". Retrieved August 23, 2010, from http://www.nei.nih.gov/health/eyediagram/index.asp. 2004.

[27] JirehDesign. "A guide to the many parts of the human eye -- how and why they work and function." Retrieved August 23, 2010, from http://www.maculacenter.com/EyeAnatomy.htm. 2007.